

Two Complementary Methods for Relative Quantification of Ligand Binding Site Burial Depth in Proteins: The ‘Cutting Plane’ and ‘Tangent Sphere’ Methods

Vicente M. Reyes, Ph.D.*

E-mail: vmrsbi.RIT.biology@gmail.com

*work done at:

Dept. of Pharmacology, School of Medicine,
University of California, San Diego
9500 Gilman Drive, La Jolla, CA 92093-0636
&
Dept. of Biological Sciences, School of Life Sciences
Rochester Institute of Technology
One Lomb Memorial Drive, Rochester, NY 14623

Abstract. We describe two complementary methods to quantify the degree of burial of ligand and/or ligand binding site (LBS) in a protein-ligand complex, namely, the ‘cutting plane’ (CP) and the ‘tangent sphere’ (TS) methods. To construct the CP and TS, two centroids are required: the protein molecular centroid (global centroid, GC), and the LBS centroid (local centroid, LC). The CP is defined as the plane passing through the LBS centroid (LC) and normal to the line passing through the LC and the protein molecular centroid (GC). The “exterior side” of the CP is the side opposite GC. The TS is defined as the sphere with center at GC and tangent to the CP at LC. The percentage of protein atoms (a.) inside the TS, and (b.) on the exterior side of the CP, are two complementary measures of ligand or LBS burial depth since the latter is directly proportional to (b.) and inversely proportional to (a.). We tested the CP and TS methods using a test set of 67 well characterized protein-ligand structures (Laskowski et al., 1996), as well as the theoretical case of an artificial protein in the form of a cubic lattice grid of points in the overall shape of a sphere and in which LBS of any depth can be specified. Results from both the CP and TS methods agree very well with data reported by Laskowski et al., and results from the theoretical case further confirm that both methods are suitable measures of ligand or LBS burial. Prior to this study, there were no such numerical measures of LBS burial available, and hence no way to directly and objectively compare LBS depths in different proteins. LBS burial depth is an important parameter as it is usually directly related to the amount of conformational change a protein undergoes upon ligand binding, and ability to quantify it could allow meaningful comparison of protein dynamics and flexibility.

Abbreviations: CP, cutting plane; TS, tangent sphere; CPM, cutting plane method; TSM, tangent sphere method; CPi, CP or CPM index; TSi, TS or TSM index; LBS, ligand binding site; GC, global or molecular centroid; LC, local or LBS centroid; lig, ligand; res, residue; sdc, sidechain; PPI, protein-protein-interaction/s; PLI, protein-ligand interaction/s; PLC, protein-ligand complex

Keywords: protein-ligand interactions; ligand burial; ligand binding site burial; protein centroid; cutting plane method; tangent sphere method; protein flexibility; protein dynamics

1 Introduction

This work was largely inspired by that of A. Ben-Shimon and M. Eisenstein in 2005. Depth of ligand burial in its cognate receptor protein is an important property of the latter biomolecule because it provides an indication of protein dynamics: deeply buried ligand binding sites imply a high degree of ligand-induced protein conformational change and hence flexibility (Rauh et al., 2004; Andersen et al., 2000). Several studies have tried to catalogue the degree of burial of active sites and have offered some generalizations relating catalytic activity with degree of ligand burial (Ben-Shimon et al., 2005). Other works focus on detecting crevices and grooves on protein surfaces, as an indirect way of locating ligand binding sites or active sites (Mitchell et al., 2001; Kawabata et al., 2007). In protein-protein complexes, on the other hand, the constituent monomers oftentimes overlap physically in the bound form, resulting from induced fit mechanism facilitated by conformational changes due to protein flexibility (Goh et al., 2004; Bui et al., 2006). There is a limit to such overlap, however: generally, the hydrophobic cores of the individual monomers are very seldom breached (Kimura et al., 2001). To the best of our knowledge, prior to this study there have been no numerical measures of LBS burial available that do not depend in protein size (i.e., relative), and hence no way to directly and objectively compare LBS depths in different proteins, although various recent works have succeeded to some degree (Tan K.P., et al. 2011; Coleman R.G. & Sharp K.A., 2010; Kalidas Y. & Chandra N., 2008; Coleman R.G. & Sharp K.A., 2006; Varrazzo D. et al., 2005; Tan K.P. et al., 2013).

Here we describe two complementary computational procedures we call the “cutting plane” and “tangent sphere” methods. The two methods are generally applicable to protein-ligand interactions (PLI) when the coordinates of residues in the ligand binding site are known, or to protein-protein interactions (PPI) if the coordinates of the residues at the PPI interface are known. In PLI, the methods are used to quantitatively determine the degree of burial of ligand binding sites in proteins (present work; see also and Reyes, V.M., unpublished [b.]), while in PPI, they may be used to quantitatively determine the degree of physical overlap between the monomer partners in the protein complex (Reyes, V.M. unpublished [c.]). The ‘cutting plane’ is then defined as that normal to the line formed by the global and local centroids, and containing the latter (Figure 1A). Another name for ‘cutting plane’ is ‘secant plane’ but we shall use the former here. The equations of the cutting plane and tangent spheres are derived from the coordinates of LC and GC. From the equation of the CP, the percentage of protein atoms on the ‘external side’ of the CP (side opposite the global centroid, purple area) may be calculated exactly and is directly proportional to the degree of burial of the ligand binding site. Likewise, from the equation of the TS, the percentage of protein atoms inside the TS (green area) may be calculated exactly and is inversely proportional to the degree of burial of the ligand binding site. The CP and TS methods find specific use in a procedure we recently developed regarding the prediction of protein-ligand interactions (Reyes, V.M. and Sheth, V.N., 2011; Reyes, V.M., unpublished [a.]) and protein-protein interaction partners (Reyes, V.M. unpublished [c.]).

2 Datasets and Methods

2.1 The Test Sets. We have used two test sets in this work: (1.) an artificial protein made up of a 3D cubic lattice of points (whose edge = 1.5 units) in the overall shape of a sphere of radius 50 units, and (2.) a set of 67 representative protein 3D structures used as a dataset in the work of Laskowski et al., 1996. We decided to apply our methods to an artificial protein (above) so that we could study its behavior in as controlled a way as possible.

2.1.1 Creating the Artificial Protein. The artificial protein was a grid of points in 3D space in the shape of a sphere with center at the origin and radius 50.0 units (Angstroms). First a 3D cubic grid of points centered at the origin with edges 100 units long ($-50.0 \leq x \leq 50.0$, $-50.0 \leq y \leq 50.0$, $-50.0 \leq z \leq 50.0$) was generated by running a Fortran program that employs a set of three nested do loops, one each for generating the x-, the y-, and the z-coordinates. The grid of points generated are separated by equal distances of 1.5 Å along the x, y and z directions. Then points lying inside the sphere with equation $x^2 + y^2 + z^2 \leq 50.0^2$ are collected. The LBS entrance is assumed to be at the ‘north pole’, i.e., at the point (0,0,50) and LBS centroids are assumed to all lie along the z- axis from (0,0,50) to (0,0,-50), and equally spaced at a constant separation of 1.0 Å, yielding a

total of 101 LBS's in all (including the one at the origin). Thus, 101 artificial proteins are created, all in the form of a spherical grid of points centered at the origin with radius 50, but differing in the location of their LBS's: the first with LBS at (0,0,50), the shallowest LBS; the second with LBS at (0,0,49), the second shallowest LBS; the third with LBS at (0,0,48), the third shallowest LBS; ...; the 99th with LBS at (0,0,-48), the third deepest LBS; the 100th with LBS at (0,0,-49), the second deepest LBS; and the 101th with LBS at (0,0,-50), the deepest LBS. These 101 artificial proteins were then analyzed using the CP and TS methods.

2.1.2 The Laskowski Data Set. This data set is composed of 67 single-chain monomeric enzymes with bound ligands, some of which contain single and others multiple bound ligands of various sizes. These proteins together with the ligands they contain are shown in Table 1 of Laskowski, et al., 1996. These proteins were selected from the 1995 PDB release based on their E.C. classifications, such that all E.C. numbers are represented once, the one with the highest resolution and best R-factor being selected. Although all are single-chain, 31 have a single domain, 30 have two domains, five have three and one has four. These 67 test structures contain varying numbers of bound ligands (from none to 11). Each was down into 1:1 protein-ligand complexes. For example, if the protein P in the structure has 4 different ligands W, X, Y and Z bound, it is broken down into four protein-ligand complexes, namely, P-W, P-X, P-Y and P-Z, corresponding to four LBSs. Thus, in all, a total of 184 LBS's were derived from this set of 67 test protein structures. It is this set of 184 LBS's that we test in this work.

2.2 The 'Cutting Plane' Method. The cutting plane method (together with the tangent sphere method) is illustrated in Figure 1A. From the coordinates of the amino acid residues making up the LBS, the LBS centroid, a local centroid (LC), may be calculated. On the other hand, the protein molecular centroid, the global centroid (GC), may be calculated from the PDB coordinate file. From these two points, the equation of the cutting plane in the form $Ax + By + Cz + D = 0$ may be determined by application of simple vector algebra as follows:

Let the local and the global centroids be the points $L(p,q,r)$ and $G(s,t,u)$. The CP is normal to line segment LG and contains L. Thus vector $\overrightarrow{LG} = \langle s-p, t-q, u-r \rangle$ is normal to the CP. For any point $Q:(x,y,z)$ on the CP, vector \overrightarrow{LQ} must be normal to vector $\overrightarrow{LQ} = \langle x-p, y-q, z-r \rangle$, which means their dot product is zero: $|\overrightarrow{LG}||\overrightarrow{LQ}|\cos 90^\circ = 0$. Since $\overrightarrow{LG} \cdot \overrightarrow{LQ} = (s-p)(x-p) + (t-q)(y-q) + (u-r)(z-r) = 0$, we have, upon rearrangement: $(s-p)x + (t-q)y + (u-r)z + D = 0$ or $Ax + By + Cz + D = 0$, where $A = s-p$, $B = t-q$, $C = u-r$ and $D = p(p-s) + q(q-t) + r(r-u)$. It can be readily shown that the global centroid is always on the positive side of the CP; hence, the percentage of protein atoms on the exterior side of the CP is readily calculated by setting $Ax + By + Cz + D \leq 0$. In Figure 1B, the behavior of the CP index (CPi; the % of protein atoms on the external side of the CP) is monitored as the LBS goes from very shallow to very deep (purple areas); the CPi increases from 0% to 100%.

2.3 The Tangent Sphere Method. The tangent sphere method (together with the cutting plane method) is illustrated in Figure 1A. Knowing the coordinates of the LBS centroid (the local centroid, LC) and the protein molecular centroid (the global centroid), the equation of the tangent sphere can be readily determined since its center is at GC and its radius is the distance between LC and GC. The percentage of protein atoms inside the TS may then be readily calculated by setting $x^2 + y^2 + z^2 \leq r^2$, where r = distance between GC and LC. As with the CP method, the TS method was done in three different ways, namely the 'sidechain submethod'; the 'residue submethod'; and the 'ligand submethod.' And similarly, results from these three submethods were very similar to each other, implying again that the submethod used does not affect the results. In Figure 1B, the behavior of the TS index (TSi; the % of protein atoms inside the TS) is monitored as the LBS goes from very shallow to very deep (green areas); the TSi decreases from 100% to 0%.

2.4 The CM-CM Method. This method is just an auxiliary method we tried to implement as an independent way to cross-check the TS and CP methods. This method is simply the determination of the distance between the GC and the LC, in Angstroms, and is a value that is expected to be inversely proportional to the LBS depth, just like the TSi. However, unlike CPi and TSi, this method does not take into consideration the percentage of protein atoms relative to the entire protein; hence this method is dependent upon the size of the protein, and is not reliable to use when the proteins being compared vary dramatically in sizes. On the contrary, CPi and TSi

are directly comparable across proteins of widely varying sizes, since they are %'s of protein atoms relative to the whole.

For thoroughness, we performed CPM and TSM in three slightly different ways depending on how the LC coordinates are calculated, namely: (1.) based on the coordinates of the atoms of the amino acid residues that contact the ligand; we designate this the 'sidechain submethod'; (2.) based on the coordinates of *all* the atoms of the amino acid residues that contact the ligand; we designate this method as the 'residue submethod': and (3.) based on the coordinates of the ligand itself, which we designate as the 'ligand submethod'. In all cases, results from these three submethods were very similar to each other, so essentially it may be concluded that the submethod used does not affect the results (data not shown).

3 Results and Discussion

3.1 Theoretical Case: The Artificial Protein. The behavior of the artificial protein under the CP and TS methods is illustrated in Figures 2, panels A, B and C. Binding sites lie along the z-axis in 1 unit increments, and the opening of the LBS is at the top, at point (0,0,50) (Figure 2A). Starting from the upper left-hand corner and following the small red arrows, we go from the artificial protein with the shallowest LBS at (0,0,50), to the one with the deepest LBS at (0,0,-50). Midway between these two extremes is the case where the LBS coincides with the protein molecular centroid (at (0,0,0)). In the first half of the graph, from the first to the 50th LBS, we note that TSi starts from 100% and decreases quickly then more slowly until it reaches a minimum at 0% (Figure 2B, blue data points); meanwhile, CPi starts from 0% and increases to a maximum at 50% (Figure 2B, pink data points). The other half of the graph, that from 51st to 101th LBS, is a mirror image of the first half, from $x=1$ to $x=50$. In this half, TSi increases from 0% to 100%, first slowly and then quickly (Figure 2B, blue data points), while CPi decreases from 50% to 0% (Figure 2B, pink data points). Note that in this case, the location of the LBS opening is known to be at (0,0,50). In this case, we can define the "anterior half" and the "posterior half" of the protein. Imagine the CP passing through the molecular centroid and cutting the protein in half; the half containing the LBS opening is the "anterior half" of the protein, while the other half (not containing the LBS opening) is its "posterior half."

Had the location of the LBS opening not been known, or known but not taken into consideration, there would have been an ambiguity in the locations of the individual LBS's as to whether they are in the anterior or posterior half of the protein. In that case, the proteins with the shallowest to deepest LBS's would have been determined based solely on their TS indices (largest to smallest) and CP indices (smallest to largest). Thus the ambiguity between the anterior and posterior halves would have caused the right half of the plot in Figure 2B (corresponding to the posterior half) to merge with the left half (corresponding to the anterior half) and the plot would have been that on Figure 2C. The TSM and CPM plots for the 67 test proteins (to be discussed shortly) in Figures 4A and 4B, respectively, correspond to this situation.

3.2 Application to the Laskowski Protein Dataset. In applying the CP, TS and CM-to-CM methods we set arbitrary limits for "shallow", "medium" (intermediate depth) and "deep" LBS predictions. For the CP method, they are: (%'s refer to % of protein atoms on the external side of CP): 0.0%-10.0% for shallow; 10.1%-20.0% for medium; and 20.1%-42.0% for deep LBS's (42% is a close upper bound for the results). For the TS method, they are (%'s refer to % of protein atoms inside the TS): 100.0%-40.1% for shallow; 40.0%-10.1% for medium; and 10.0%-0.0% for deep LBS's. For the CM-to-CM method, they are (Å's refer to the distance between the global centroid, GC, and the local centroid, LC): 38.0Å - 15.1Å for shallow; 15.0 Å-10.1Å for medium; and 10.0Å -0.0Å for deep LBS's. These were the best limit values as judged from the frequency distributions obtained, as discussed below.

3.2.1 The Tangent Sphere Method as Applied to the Laskowski Dataset. We first determined the frequency distribution of the prediction results (i.e., "shallow", "intermediate" and "deep") from the TS method, using the ligand, residue and sidechain submethods described earlier. From the distributions (Figure 3A.1, 3A.2 and 3A.3, respectively), it may be concluded that the TS method has more resolving power at the lower bins (shallow LBS's) than at the higher bins (deep LBS's), indicating that it has higher specificity for shallow LBS's than to deep LBS's.

Figure 4A shows the results from the TS method from the 3 submethods: ligand (blue data points), residue (pink data points) and sidechain (yellow data points) submethods. All show the same trend in going from shallow to deep LBS's: decreasing rather quickly in the first half, then more slowly on the second half, almost plateauing near 0% towards the deepest LBS's. We note that this is very similar to the behavior of the artificial protein in Figure 2C (blue data points) and the first half of the plot in Figure 2B (blue data points).

Let us go back to the concept of “anterior” and “posterior” halves of a protein. These are both illustrated in the central object in Figure 1B. In the case of the artificial protein, the researcher knows the exact location of the LBS in relative to the LBS opening, hence it is possible to accurately arrange the proteins from those that have shallowest LBS's (in the anterior half) to those that have deepest LBS's (in the posterior half). In actual work as well in our application to the Laskowski dataset, however, the LBS opening is either unknown or known but not taken in consideration due to automation of the process. Thus in these cases, it is not possible to differentiate the LBS's lying in the anterior half from those that lie in the posterior half. Thus there is such ambiguity in the case of the Laskowski test proteins (where the LBS opening may have been known, but not taken it into account because of automation).

3.2.2 The Cutting Plane Method as Applied to the Laskowski Dataset. As in the TS method, we determined the frequency distribution of the prediction results (i.e., “shallow”, “intermediate” and “deep”) using the ligand, residue and sidechain submethods described earlier. From the distributions (Figure 3B.1, 3B.2 and 3B.3, respectively), it may be concluded that the CP method has more resolving power at the higher bins (deep LBS's) than at the lower bins (shallow LBS's), indicating that it has higher specificity for deep LBS's than to shallow LBS's. This is opposite behavior to that of the TS method.

Figure 4B shows the results from the CP method from the 3 submethods: ligand (blue data points), residue (pink data points) and sidechain (yellow data points) submethods. All show the same trend in going from shallow to deep LBS's: increasing rather slowly at first, then faster and almost linearly thereafter, towards the deeper LBS's, and then stops at between 39% and 44% at the deepest LBS's. We note that this is very similar to the behavior of the artificial protein in Figure 2C (pink data points) and the first half of the plot in Figure 2B (pink data points).

As was explained in the previous section, there is an ambiguity in the latter case. However, as can be seen from Figure 4A, the CP results do not reach 50 but stops between 39%, 40% and 44% for the sidechain, ligand and residue submethods, respectively. This means that the LBS's do not reach the depth of the protein molecular centroid. Therefore it is reasonable to conclude that there are no LBS's on the posterior half of the protein, i.e., all LBS's are in the anterior half. This must be so since it is quite improbable that no LBS's are found on and around the global centroid while LBS's on the posterior half exist. As for the case of the TS method in Figure 4B, we see that it does reach 0% near the deepest LBS's (0.0%, 0.15% and 0.25% for the ligand, residue, and sidechain methods, respectively). However, as was discussed earlier, the TS method has low resolving power for the deep LBS's and in fact the curve plateaus near at 0% near the deepest LBS's. The TS method seems unable to differentiate between LBS depths when the TS reaches a radius of within 5 Å from the global centroid. This appears to validate our conclusion that there are probably no LBS's on the posterior halves of the 67 test proteins.

3.2.3 The CM-to-CM Method. Figure 3C.1, 3C.2 and 3C.3 show the frequency distribution of the results from the CM-to-CM method, using the ligand submethod, residue submethod and sidechain submethod, respectively. Here, the horizontal axis is the distance in Angstroms between the local CM and the global CM (“CM-to-CM value”), going from shallowest LBS at 38 Å on the extreme left, to deepest LBS at 0 Å on the extreme right, partitioned into intervals of width 1.9 Å, for a total number of intervals (“bins”) of 20. The vertical axis is the number of LBS's (out of the 184 total) with CM-to-CM values corresponding to each interval or bin along the x-axis. For example, in the CM-to-CM method, ligand submethod, there is 1 LBS with a CM-to-CM value between 38 Å and 36.1 Å (first bin), while there are no LBS's with a CM-to-CM value between 1.9 Å and 0% (last bin). Note that the resolving power of the CM-to-CM method is highest on the first half of the plot (shallow LBS's), dipping to a minimum about halfway through the second half, and then increases again

towards the end of the second half (very deep LBS's), indicating that it has higher specificity for shallow to almost-shallow LBS's and for very deep LBS's.

Figure 4C shows the results from the CM-to-CM method from the 3 submethods: ligand (blue data points), residue (pink data points) and sidechain (yellow data points) methods. All show the same trend in going from shallow to deep LBS's: decreasing rather quickly in the first quarter, then more slowly on the second and third quarters, then more slowly again and almost plateauing near 0% towards the deepest LBS's. That there are most probably no LBS's on the posterior halves of the 67 test proteins is also supported by these CM-to-CM data since the LC to GC distance does not reach 0 Å (3.0 Å, 1.9 Å and 2.4 Å for the ligand, residue and sidechain submethods, respectively). This implies, as in the CP method, that no LBS is close to the GC, hence there are probably no LBS's in the posteriori half of the proteins.

3.3 Summary of Final Results. From the 67 Laskowski dataset of protein structures, there are a total of 184 LBS's since some of the proteins in the dataset have more than one ligand (from as low as none to as many as 11; see Table 1 and legend), as mentioned earlier. The determination of the mutual intersections of the shallow, medium (intermediate depth) and deep predictions by the TSM, CPM and CM-CM method, using the 3 submethods (ligand, residue and sidechain submethods), respectively, have been determined, and the results are shown and summarized in the Venn Diagrams in Figure 5, panels A, B and C for the TSM, CPM and CM-CM methods, respectively, and similarly in Figure 6, panels A, B and C. The overall results from the TSM, CPM and CM-CM are presented in combined form in Figure 7, Panel A while in Panel B, only the combined results from the TSM and CPM are presented (with the CM-CM results excluded).

Specifically, Figure 5A, B and C show the first step in the analysis process, which is the pairwise determination of the intersections among the three submethods (ligand, residue and sidechain) in the TSM, CPM and CM-CM methods, respectively. Meanwhile, Figure 6A, B and C show the second step in the process, which is the determination of the mutual 3-way intersections among the three submethods (ligand, residue and sidechain) in the TSM, CPM and CM-CM methods, respectively. Figure 7 shows the final step in the analysis process. In Panel A, the determination of the mutual three-way intersections among the TSM, CPM and CM-CM methods are shown. In this case, 37 structures are common to the TS, CP and CM-to-CM shallow LBS predictions, 8 are common to the medium LBS predictions, and finally 47 are common to the deep LBS predictions. The identities of these 37 shallow, 8 medium and 47 deep LBS's are shown in Table 2. Thus a total of $37+8+47 = 92$ LBS's out of the 184 LBS's, or 50%, were predicted identically by our three methods, TS, CP and CM-CM. Panel B is the same as Panel A except that the CM-CM results are excluded, as this method is disfavored relative to the TSM and CPM methods because it (the CM-CM method) is dependent on protein size, while the TSM and CPM are not. In this case, 38 structures are common to the TSM and CPM shallow LBS predictions, 11 are common to the medium LBS predictions, and finally 51 are common to the deep LBS predictions. The identities of these 38 shallow, 11 medium and 51 deep LBS's may be gleaned from Table 2. Thus a total of $38+11+51 = 100$ LBS's out of the 184 LBS's, or 54%, were predicted identically by the two methods about which this work is about, the TS and CP methods. Note that an additional 1, 3 and 4 LBSs are included in the shallow, medium and deep predictions, respectively compared to the previous tabulation. These additional LBSs represent the ones which were supposed to have been incorrectly predicted by the CM-CM method due to its dependence on protein size.

Finally in Table 3, panels A, B and C, we show the identities and the corresponding CP_i and TS_i values of the final predictions in Figure 7A and B. Panel A show the deep predictions, panel B the medium predictions, and panel C the shallow predictions. Note that the CP_i 's of the LBSs in panels A, B and C decrease in that order, while the TS_i 's increase in the same order. These results demonstrate the complementarity between these two LBS burial depth metrics. To the best of our knowledge, prior to this study, no such (numerical) metrics existed for LBS burial depth. With these two new metrics (TS_i and CP_i), LBS burial depth in different proteins, regardless of size variations among them, may be compared.

The results we obtained above are very similar to the results described by Laskowski et al. (1996), wherein the ligand depths were determined by manual (visual) inspection. Hence we conclude that the Cutting Plane (CP) and Tangent Sphere (TS) methods are quite effective and reliable methods of determining and quantifying

ligand or LBS burial in proteins, provided that the coordinates of the LBS (local site) and that of the entire protein molecule (global structure) are available.

3.4 Advantages and Limitations of the Methods. Prior to this study, there were no numerical measures of LBS burial available that do not depend in protein size, and hence no way to directly and objectively compare LBS depths in different proteins. The CP and TS methods are two complementary methods that provide such a way. The fact that the TS and CP indices are complementary does not mean that they are redundant in the sense that if one is known, the other may be precisely calculated; that is only true for a perfectly spherical protein, but real proteins are never perfectly spherical. That being said, the CP and TS methods would work best if the test protein is roughly spherical, or globular, in shape. If the protein has an overall concavity, or is otherwise irregular in shape, the method becomes less accurate. Thus, we can expect the CP and TS methods to be less accurate for rod-shaped proteins, etc. But since the majority of structurally solved proteins (about 80% of them) are globular (“spheroproteins”), it may be concluded that the CP and TS methods are generally applicable. The complementarity of the two methods (i.e., the CP index is directly proportional to LBS burial depth, while the TS index is inversely proportional to it) is an advantage of employing both methods in parallel since they cross-validate each other. Although TSM and CPM were created out of a need for validating our own results from our prediction studies (Reyes, V.M., unpublished [a.], [b.] and [c.]), it is generally applicable to **any** protein whose atomic coordinates, as well as those of the relevant local sites in it (i.e., LBSs), are known.

4 Conclusions.

We have developed a couple of complementary methods, as well as an auxiliary method, to quantify the depth of burial of a ligand or its binding site in a protein structure. These methods, called the “Cutting Plane,” the “Tangent Sphere” and the “Centroid-to-Centroid” methods, respectively, are all implemented as Fortran 77/90 programs and are fast, efficient and amenable to high-throughput or big-batch applications. We tested the methods on a set of 67 previously characterized structures containing a combined total of 184 LBS’s, as well as on an artificial protein consisting of a grid of points in the shape of a sphere, where LBS’s can be arbitrarily assigned anywhere on it. Predictions on the LBSs by the three methods in the form of “shallow”, “medium” (intermediate depth) and “deep” are in line with previous characterizations done by human visual inspection. The predictions are also independent of protein size, as they are relative to the size of the entire protein (based on percentages of portions of protein relative to the whole). We believe that these methods may find useful applications in structural proteomics, especially protein dynamics, as ligand burial depth is indicative of the amount of conformational changes the protein undergoes in binding the ligand. To the best of our knowledge, this work is the first attempt at the relative quantification of the depth of burial of ligand or ligand binding sites in proteins using cutting planes and tangent spheres as described in this work.

Acknowledgments. This work was supported by an Institutional Research and Academic Career Development Award to the author, NIGMS/NIH grant number GM 68524. The author thanks Ms. Srujana Cheguri, one of his M.S. Bioinformatics graduate students at Rochester Institute of Technology (RIT), for verifying results. The author wishes to acknowledge the San Diego Supercomputer Center, the UCSD Academic Computing Services, and the UCSD Biomedical Library, for the help and support of their staff and personnel. He also acknowledges the Division of Research Computing at RIT, and computing resources from the Dept. of Biological Sciences, College of Science, at RIT.

References:

Andersen JF, Ding XD, Balfour C, Shokhireva TK, Champagne DE, Walker FA, Montfort WR. “Kinetics and equilibria in ligand binding by nitrophorins 1-4: evidence for stabilization of a nitric oxide-ferriheme complex through a ligand-induced conformational trap.” *Biochemistry*. 2000 Aug 22;39(33):10118-31.

- Ben-Shimon, A., and Eisenstein, M. 2005. Looking at enzymes from the inside out: the proximity of catalytic residues to the molecular centroid can be used for detection of active sites and enzyme-ligand interfaces. *J Mol Biol.* **351**:309-26.
- Bui JM, McCammon JA. "Protein complex formation by acetylcholinesterase and the neurotoxin fasciculin-2 appears to involve an induced-fit mechanism." *Proc Natl Acad Sci U. S. A.* 2006 Oct 17;103(42):15451-6. Epub 2006 Oct 4.
- Coleman RG, Sharp KA. (2010) Protein pockets: inventory, shape, and comparison. *J Chem Inf Model.* 2010 Apr 26;50(4):589-603. doi: 10.1021/ci900397t.
- Coleman RG, Sharp KA. (2006) Travel depth, a new shape descriptor for macromolecules: application to ligand binding. *J Mol Biol.* 2006 Sep 22;362(3):441-58. Epub 2006 Jul 15.
- Goh CS, Milburn D, Gerstein M. "Conformational changes associated with protein-protein interactions." *Curr Opin Struct Biol.* 2004 Feb;14(1):104-9.
- Goodman, JE & O'Rourke, J. (eds.) In: "Handbook of Computational Geometry", 2nd ed., © 2004, Chapman & Hall Pub. Co., Boca Raton, FL
- Kalidas Y, Chandra N. (2008) PocketDepth: a new depth based algorithm for identification of ligand binding sites in proteins. *J Struct Biol.* 2008 Jan;161(1):31-42. Epub 2007 Sep 15.
- Kawabata T, Go N. "Detection of pockets on protein surfaces using small and large probe spheres to find putative ligand binding sites." *Proteins.* 2007 Apr 19; [Epub ahead of print]
- Kimura SR, Brower RC, Vajda S, Camacho CJ. "Dynamical view of the positions of key side chains in protein-protein recognition." *Biophys J.* 2001 Feb;80(2):635-42.
- Laskowski, RA, Luscombe, NM, Swindells MB and Thornton JM (1996) "Protein clefts in molecular recognition and function", *Protein Sci.*, 5: 2438-2452
- Mitchell, J.C., Kerr, R. and Ten Eyck, L.F. (2001) "Rapid Atomic Density Methods for Molecular Shape Characterization," *J. Mol. Graph. Model.* 19(3): 324-329.
- Rauh D, Klebe G, Stubbs MT. "Understanding protein-ligand interactions: the price of protein flexibility." *J Mol Biol.* 2004 Jan 30;335(5):1325-41.
- Reyes, V.M. & Sheth, V.N., "Visualization of Protein 3D Structures in 'Double-Centroid' Reduced Representation: Application to Ligand Binding Site Modeling and Screening", 2011, *Handbook of Research in Computational and Systems Biology: Interdisciplinary Approaches*, IGI-Global/Springer, pp. 583-598.
- Reyes, V.M. (unpublished [a.]) "An Automatable Analytical Algorithm for Structure-Based Protein Functional Annotation via Detection of Specific Ligand 3D Binding Sites: Application to ATP Binding Sites in ser/thr Protein Kinases and GTP Binding Sites in Small Ras-type G-Proteins" (forthcoming); Abstract: *J. Biomol. Struct. & Dyn.*, Book of Abstracts, Albany 2009: The 16th Conversation, June 16-20, 2009, Vol. 26 (6) June 2009, p. 874
- Reyes, V.M. (unpublished [b.]) "Structure-Based Prediction of Sialic Acid, Retinoic Acid and Heme-Bound and Unbound Nitric Oxide Protein Binding Sites" (forthcoming); Abstract: *J. Biomol. Struct. & Dyn.*, Book of Abstracts, Albany 2009: The 16th Conversation, June 16-20, 2009, Vol. 26 (6) June 2009, p. 874
- Reyes, V.M. (unpublished [c.]) "A Novel, Automatable and Analytical (Exact) Method for Structure-Based Prediction of Protein-Protein Interaction Partners" (forthcoming); Abstract: *J. Biomol. Struct. & Dyn.*, Book of Abstracts, Albany 2009: The 16th Conversation, June 16-20, 2009, Vol. 26 (6) June 2009, p. 873

Tan KP, Nguyen TB, Patel S, Varadarajan R, Madhusudhan MS. (2013) Depth: a web server to compute depth, cavity sizes, detect potential small-molecule ligand-binding cavities and predict the pKa of ionizable residues in proteins. *Nucleic Acids Res.* 2013 Jul;41(Web Server issue):W314-21. doi: 10.1093/nar/gkt503. Epub 2013 Jun 12.

Tan KP, Varadarajan R, Madhusudhan MS. (2011) DEPTH: a web server to compute depth and predict small-molecule binding cavities in proteins. *Nucleic Acids Res.* 2011 Jul;39 (Web Server issue):W242-8. doi: 10.1093/nar/gkr356. Epub 2011 May 16.

Tronrud DE. (1997) "TNT refinement package." *Methods Enzymol.* 277:306-19.

Varrazzo D, Bernini A, Spiga O, Ciutti A, Chiellini S, Venditti V, Bracci L, Niccolai N. (2005) Three-dimensional computation of atom depth in complex molecular structures. *Bioinformatics.* 2005 Jun 15;21(12):2856-60. Epub 2005 Apr 12.

FIGURE LEGENDS:

Figure 1, Panel A: Definition and Illustration of the Cutting Plane and Tangent Sphere Methods

Illustration of the Cutting Plane and Tangent Sphere Methods and how they complement each other. The brown circle represents a spherical protein, with a ligand binding site whose opening is at the top; the ligand is shown as a small red circle. The blue horizontal line is the cutting plane (CP), cutting the protein through its ligand binding site (LBS) centroid. This centroid is different from the protein molecular centroid, shown at the center of the protein as a ©: the former is a local centroid, while the latter is a global centroid. The tangent sphere (TS) is shown as a green circle tangent to the CP at the LBS centroid. The exterior side of the CP is defined to be the side opposite the protein molecular centroid, while its interior side is that containing the protein molecular centroid. The volume of the protein lying on the CP exterior side is shown in purple, while the volume of the protein lying inside the TS, on the interior side of the CP, is shown in green.

Panel B: Illustration of the CP and TS Methods on a Artificial Protein in the form of a Sphere. To start with, the protein is shown with a shallow ligand binding site. The CP (blue line) and TS (green circle) are shown as well, and the volume of the protein lying on the exterior of the CP and in the interior of the TS are shown in purple and green, respectively. These volumes, expressed as percentages of the total protein volume, are also shown above (%CP) and below (%TS) the cutting plane, respectively; we designate them as the CP and TS indices, respectively. In the succeeding panels, the LBS is made deeper and deeper into the protein; the behavior of %CP and %TS follow two different trends and are discussed in the text and plotted in Figure 3. In both panels, the V-shaped concavity in the circle represents the LBS, but shown only for purposes of illustration. In all our calculations, the receptor protein is conceptualized as a perfect sphere without any such concavity embodying the LBS.

Figure 2: Plots of CPM and TSM Results for the Theoretical Case ("Artificial Protein")

Panel A: The artificial protein is shown as a spherical grid of points with center at the origin and the LBS assumed to be at the "top" i.e., at its maximum point along the positive z-axis. Plots of the CP and TS indices for this case where the LBS opening is precisely known is shown in Panel B. Plots of the CP and TS indices for the case where the LBS opening is **not** known is shown in Panel C.

Panel B: %CP and %TS data from the artificial protein as LBS is made to vary from very shallow (near the surface), to shallow, to deep, to very deep (near the protein centroid), to deepest (near the other end of the protein opposite the LBS opening). The %CP (pink data points) and the %TS (dark blue data points) were plotted against the LBS depth, with the shallowest on the far left and the deepest on the far right. LBS depth exactly midway between the shallowest and deepest depths corresponds to the situation where the LBS is at or very near the protein molecular centroid. See text for a discussion of the %CP and %TS trends as LBS depth varies.

Panel C: This is what the plot in Panel A would look like if the LBS opening is unknown in the case of the artificial proteins. The right half of the plot will fold into the left half due to the resulting ambiguity between the

anterior and posterior halves of the proteins (see text). This figure shows a basic difference between the artificial proteins and the 67 test proteins. In the artificial proteins the location of the LBS opening is known, and there are LBS's on both the anterior and posterior half of the protein. In the test (real) proteins, the location of the LBS opening is not known, hence there is ambiguity between the anterior half and the posterior half of the proteins in terms of the location of the LBS's. However, data from the CP and CM-to-CM methods indicate that there are no LBS's on the posterior half of the proteins; data from the TS method does not disagree with such conclusion.

Figure 3: Frequency Distribution Plots for CPM, TSM and CM-CM Methods for the 67 Test Structures

Panels A1, A2 and A3: Frequency distribution of the classification results obtained from the Tangent Sphere method using the three submethods: ligand CM (Panel A1), residue CM (Panel A2), and side chain CM (Panel A3). In the TS method, the LBS depth is measured in terms of the fraction of protein volume lying inside the tangent sphere, and the range of this parameter is (theoretically and experimentally) from 1% to 100% (see text). Each bin or interval on the horizontal axis is 5% in all 3 panels, giving rise to 20 bins. The vertical axes measure the number of structures in each particular bin. Note that TSM has higher resolving power for shallower LBSs than for deeper LBSs.

Panels B1, B2 and B3: Frequency distribution of the classification results obtained from the Cutting Plane method using the three submethods: ligand CM (Panel B1), residue CM (Panel B2), and side chain CM (Panel B3). In the CP method, the LBS depth is measured in terms of the fraction of protein volume on the external side of the cutting plane, and the range of this parameter is theoretically from 0% to 50%, but experimentally the upper bound only goes to 42% (see text). Each bin or interval on the horizontal axis is 2.1% in all 3 panels, giving rise to 20 bins. The vertical axes measure the number of structures in each particular bin. Note that CPM has higher resolving power for deeper LBSs than for shallower LBSs.

Panels C1, C2 and C3: Frequency distribution of the classification results obtained from the CM-CM method using the three submethods: ligand CM (Panel C1), residue CM (Panel C2), and side chain CM (Panel C3). In the CM-to-CM method, the LBS depth is measured in terms of the distance between the local and the global centroids (LBS and protein CM's, respectively), and the range of this parameter is from 0 Å (local and global CM's coincide), and there is no theoretical upper bound, but in this data set, the upper bound is 38 Å (see text). Each bin or interval on the horizontal axis is 1.9 Å in all 3 panels, giving rise to 20 bins. The vertical axes measure the number of structures in each particular bin. Note that the maximal resolving power of the CM-CM method is intermediate to those of the TS and CP methods.

Figure 4: Plots of CPM and TSM Results for the 67 Test Structures

Panel A: Results of LBS depth quantification using the CP method done using the 3 submethods, ligand CM (black), residue CM (pink) and side chain CM (yellow). LBS depth is directly proportional to % protein atoms on the external side of the CP, with a lower bound of 0%, and an upper bound of about 42%. Along the horizontal axis are the 184 protein-ligand pairs from the Laskowski dataset arranged from those with lowest CP index (leftmost) to those with highest CP index (rightmost).

Panel B: Results of LBS depth quantification using the TS method done using the 3 submethods, ligand CM (black), residue CM (pink) and side chain CM (yellow). LBS depth is inversely proportional to % protein atoms lying inside the TS, with a lower bound of about x%, and an upper bound of about 42%. Along the horizontal axis are the 184 protein-ligand pairs from the Laskowski dataset arranged from those with highest TS index (leftmost) to those with lowest TS index (rightmost).

Panel C: Results of LBS depth quantification using the CM-CM method done using the 3 submethods, ligand CM (black), residue CM (pink) and side chain CM (yellow). LBS depth is inversely proportional to the distance between the global and the local centroids, and in this data set, this parameter has a lower bound of about 2 Å and an upper bound of about 38 Å. Along the horizontal axis are the 184 protein-ligand pairs from the Laskowski dataset arranged from those with largest CM-CM distance (leftmost) to those with smallest CM-CM distance (rightmost).

Figure 5A,B,C: Summary Two-Way Venn Diagrams. Nine Venn Diagrams showing pairwise intersections of the results from the ligand, residue and side chain submethods for those structures classified as “deep”, “medium (intermediate depth), and “shallow.” Data in panel A are from the TS method, those in panel B from the CP method, and those in panel C from the CM-CM method.

Figure 6A,B,C: Summary Three-Way Venn Diagrams. Three Venn Diagrams showing the mutual (three-way) intersections of the results from the ligand, residue and side chain submethods for those structures classified as “deep”, “medium”, and “shallow”. Data were derived from those in Figure 5, panels A, B and C. The entries in the center of each Venn Diagram are the 3-way intersections among the three submethods (ligand, residue and side chain). Data in panel A are from the TS method, those in panel B from the CP method, and those in panel C from the CM-CM method.

Figure 7, Panel A: Venn Diagrams Illustrating Commonalities of Prediction by the CP, TS and CM-CM Methods. The final results from the TS, CP and CM-CM methods of determining LBS burial depth is shown. The top Venn Diagram shows the intersections of the “shallow” predictions by these three methods, and we see that 37 are common among them. The lower left Venn Diagram shows the intersections of the “medium” (i.e., intermediate LBS depth) predictions of these three methods, and we see that 8 are common among them. The lower right Venn Diagram shows the intersections of the “deep” predictions of these three methods, and we see that 47 are common among them. In all 92 cases ($=37+8+47$), the predictions were identical with those of Laskowski et al. (1996), whose assessments were derived by inspection (visual).

Panel B: If the CM-CM results are not considered, we arrive at the Venn Diagram shown here. The common intersection will then be 100 ($=38+11+51$) instead of 92. The CM-CM method is oftentimes best left out because it is dependent on protein size, since it measures absolute distances in Angstroms instead of percentages of atoms in the protein (relative to that in the entire molecule) as the TS and CP indices do.

TABLE LEGENDS:

Table 1: Tabulation of the 67 Test Structures from the Laskowski Dataset. Many of the 67 structures (column 1) have more than one bound ligand; each was broken down into 1:1 protein-ligand pairs. For example, consider a structure that has a single protein chain P, with 3 bound ligand molecules, A, B and C. This structure is broken down into P-A, P-B and P-C, and the 1:1 protein-ligand pairs are designated 1, 2 and 3. If a structure contains a single ligand, the protein-ligand pair is designated “0”. These are the entries in the third column of the table. Broken down in this way, the 67 structures in the Laskowski data set gave rise to 184 protein-ligand pairs. The second column of the table are the short-hand designations of the 67 structures. For example, “Bl.lig4” would refer to structure with PDB ID “1ELA” and its ligand “ACY” in chain B, residue number 300; “Bl.lbs4” would mean the same, except that the ligand binding site, not the ligand, is the entity on question.

Table 2: LBS’s Judged “Shallow”, Medium depth”, and “Deep” by the Three Methods. These are the identities of the 1:1 protein-ligand pairs classified as “shallow”, “medium”, and “deep” by the 3 methods as shown in the center of each Venn Diagrams in Figure 6, panels A B and C, respectively. The first 3 columns show the results from the TS method, the next three from the CP method, and the last three from the CM-CM method. Each column is the mutual (three-way) intersection of the ligand, residue and side chain submethods for each pertinent classification (deep, medium and shallow) and method (TS, CP and CM-CM).

Table 3A,B,C: TS and CP Indices of Common Predictions. The TS indices (first 4 columns), CP indices (next 4 columns) and CM-to-CM distances (last 4 columns) of the Laskowski structures classified as “deep” (panel A), “medium” (panel B), and “shallow” (panel C). In each panel, the three indices from the three submethods (ligand, “lig”; residue, “res”; side chain, “sdc”; average, “ave”) are shown in black, and their averages are shown in red. The numbers in blue (8 in all) in the average column of the CM-CM section are the ones that become excluded if the CM-CM method is not considered (see Figure 7A,B), for reasons discussed previously. These indices (the TS and CP indices, in particular.) are precisely the quantitative measures of LBS burial that are referred to in the text. Prior to this study, there were no such numerical measures of LBS burial available, and hence no way to directly and objectively compare LBS depths in different proteins.

FIGURES:

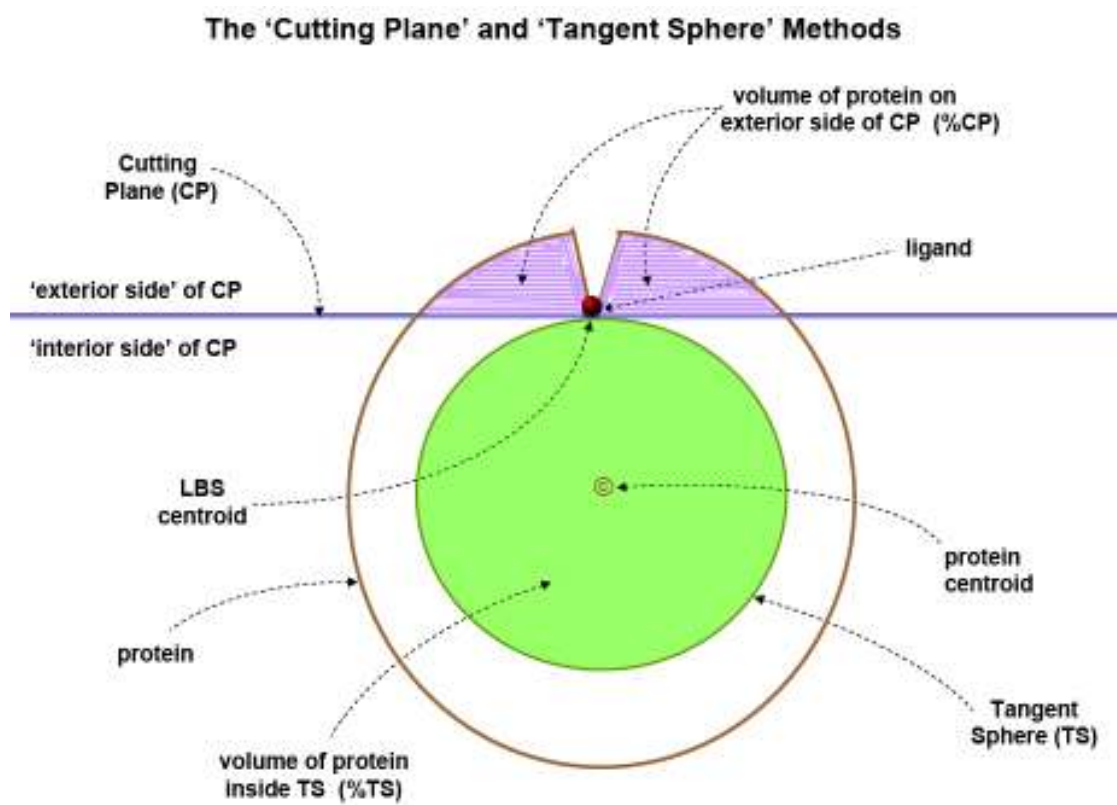


Figure 1A

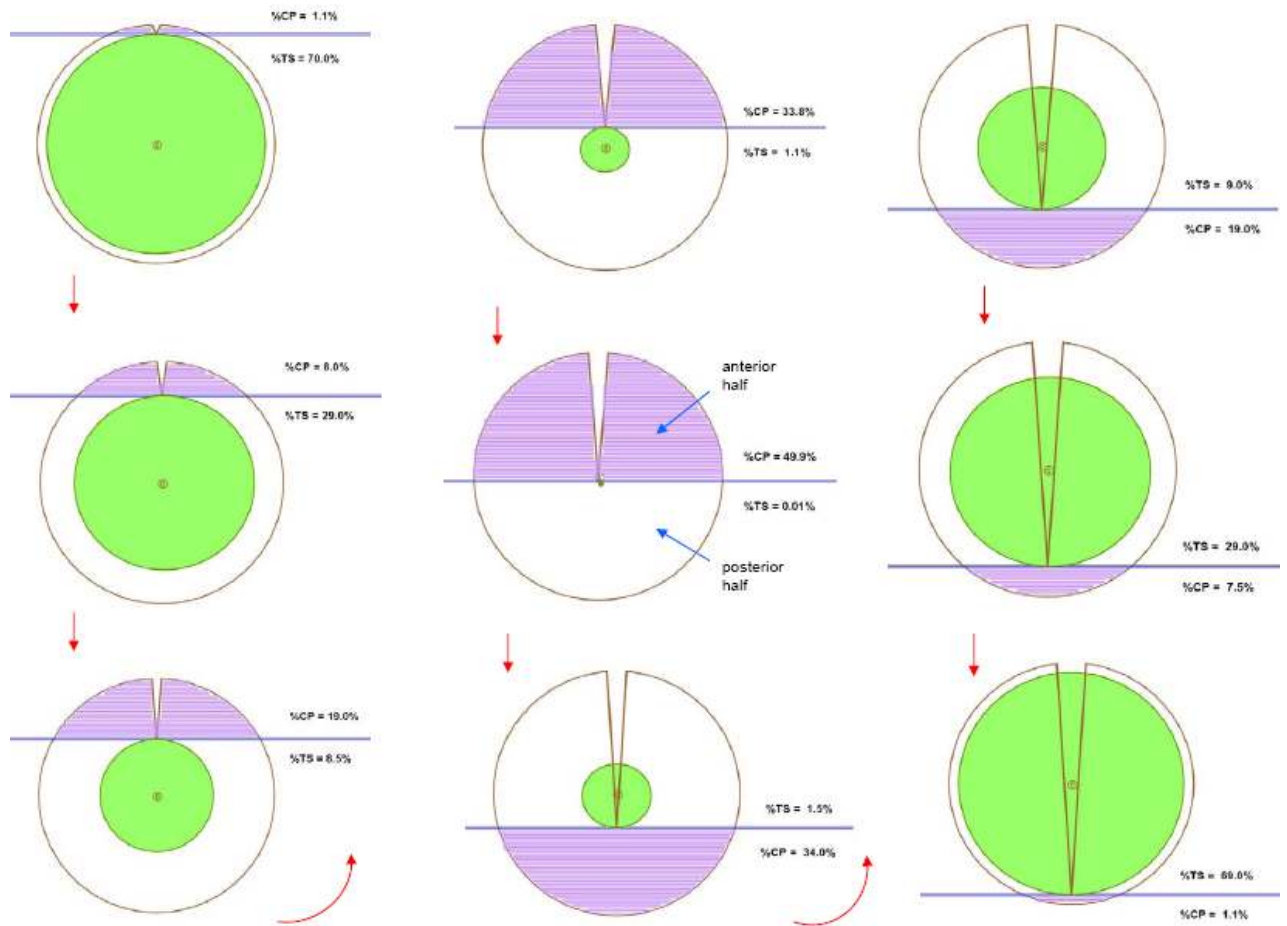


Figure 1B

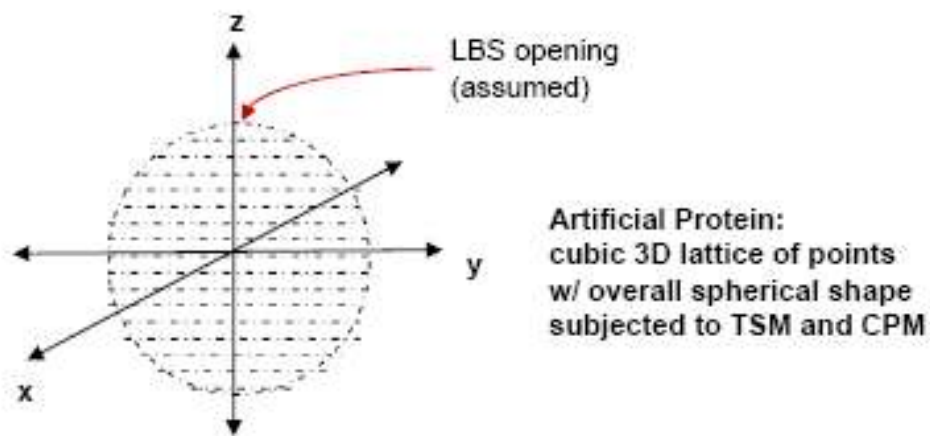


Figure 2A

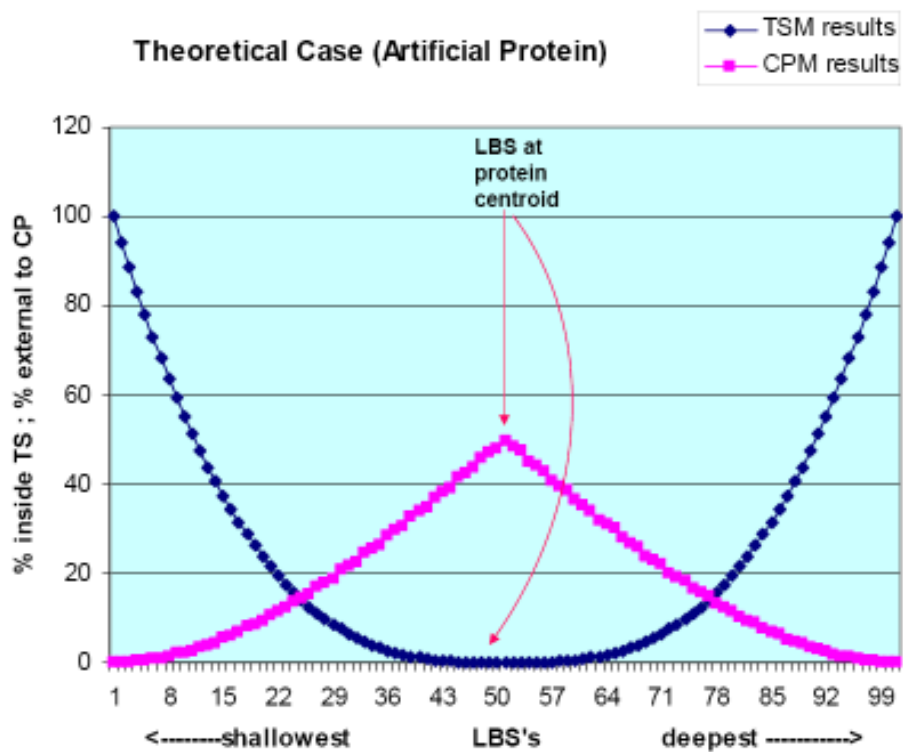


Figure 2B

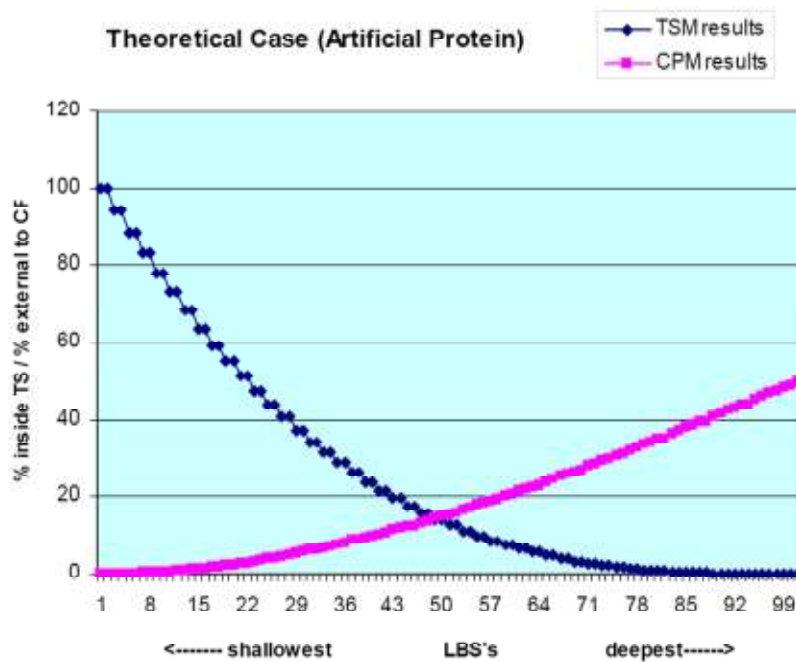


Figure 2C

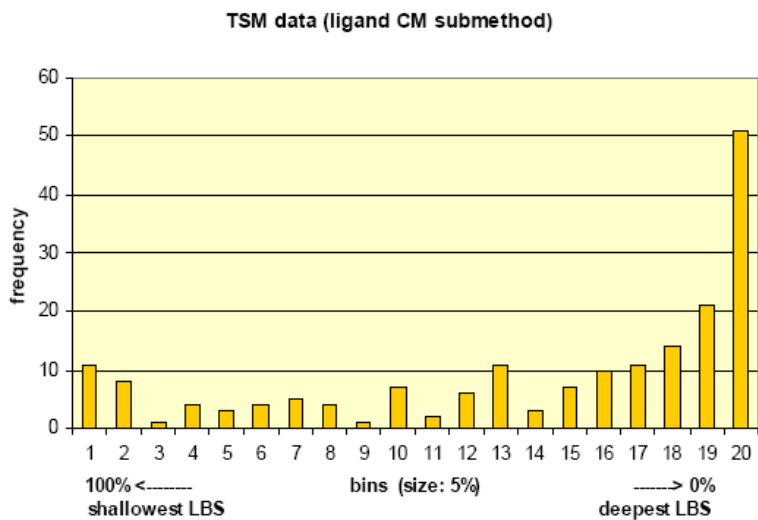


Figure 3A.1

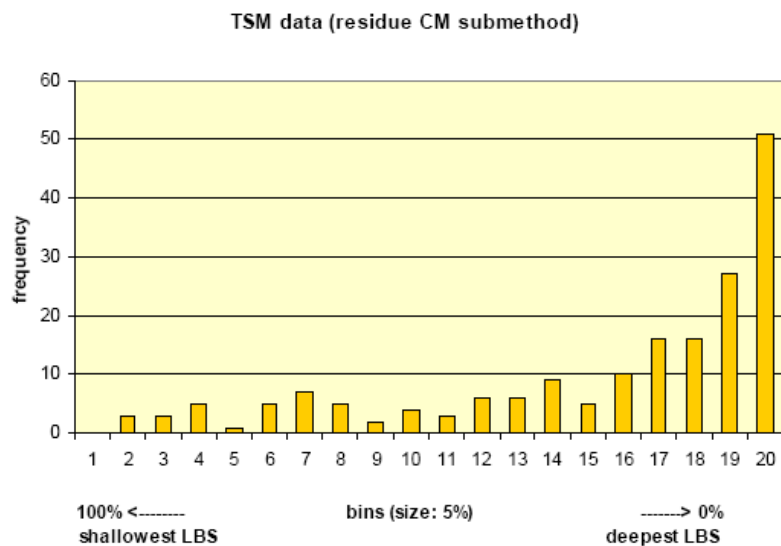


Figure 3A.2

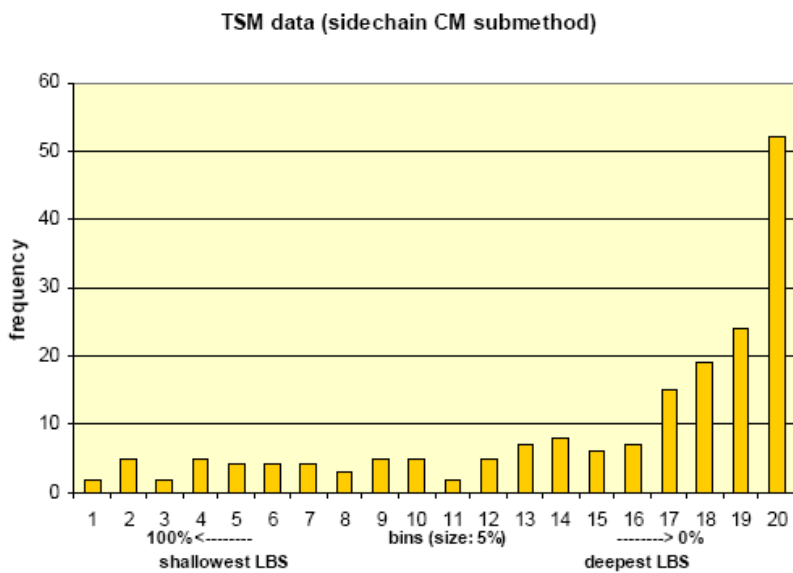


Figure 3A.3

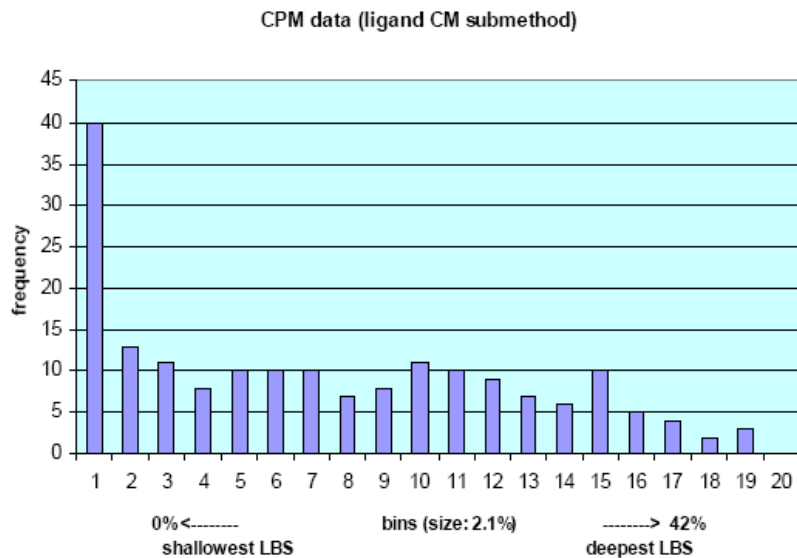


Figure 3B.1

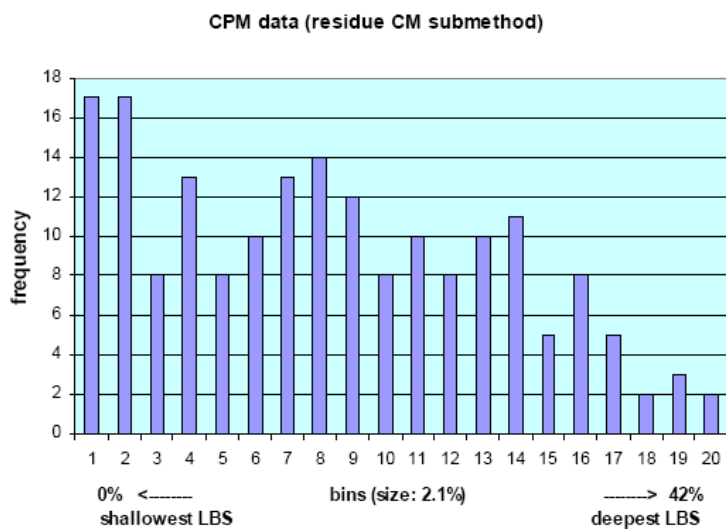


Figure 3B.2

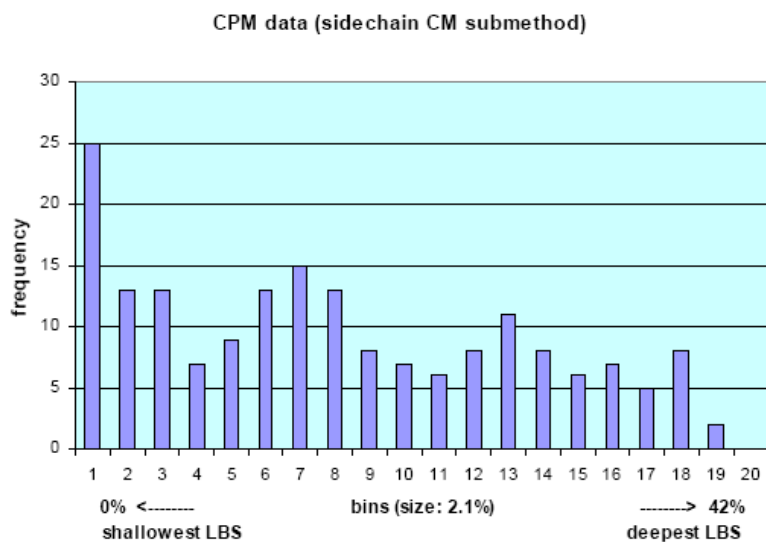


Figure 3B.3

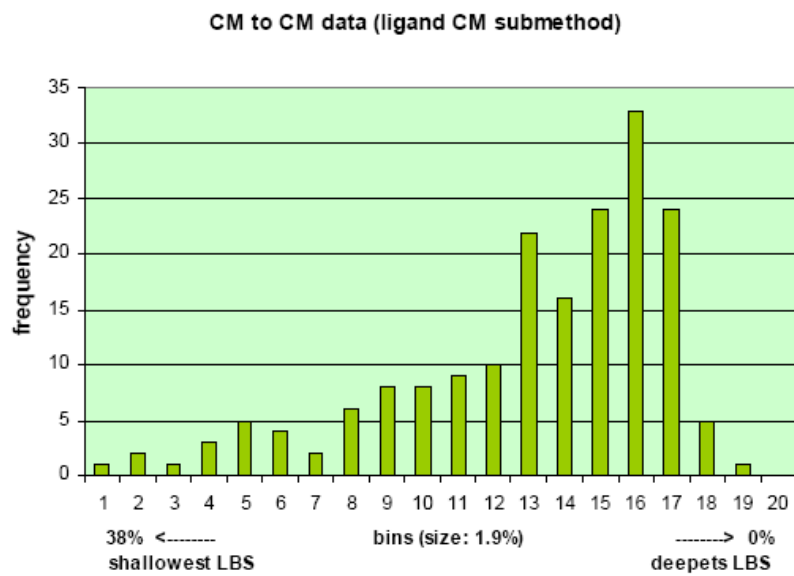


Figure 3C.1

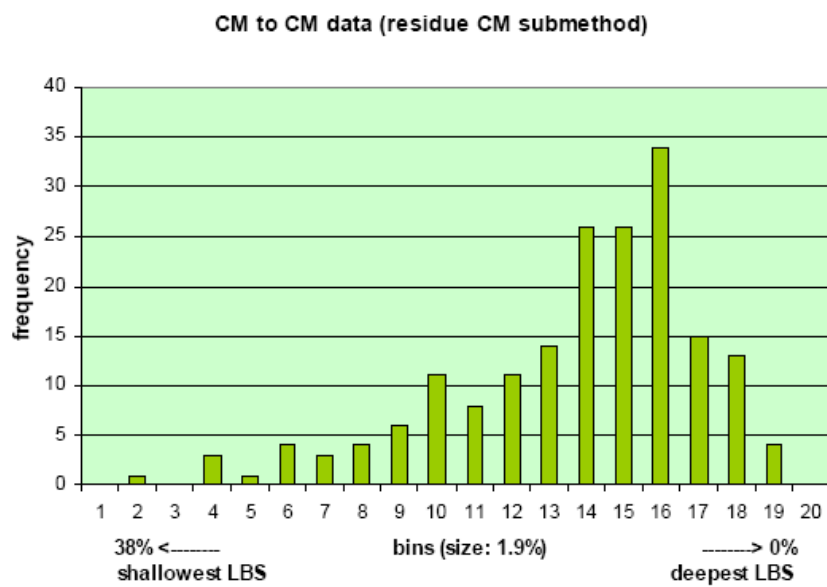


Figure 3C.2

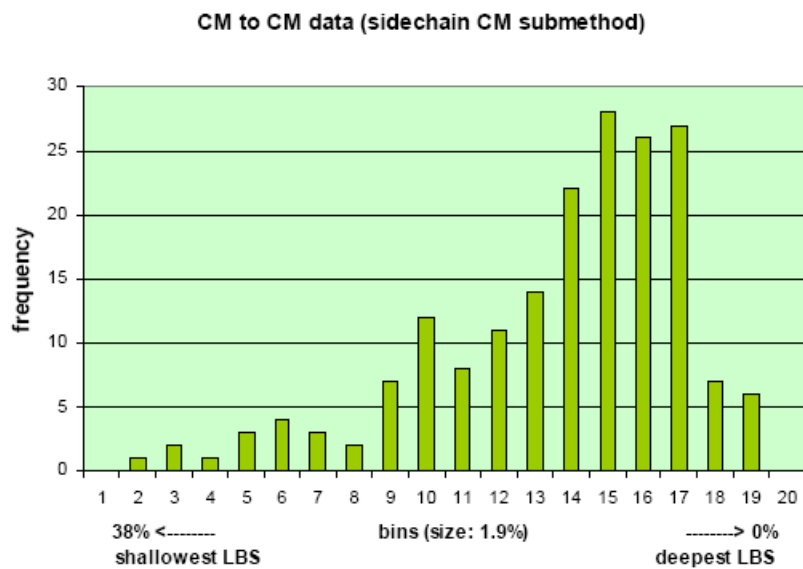


Figure 3C.3

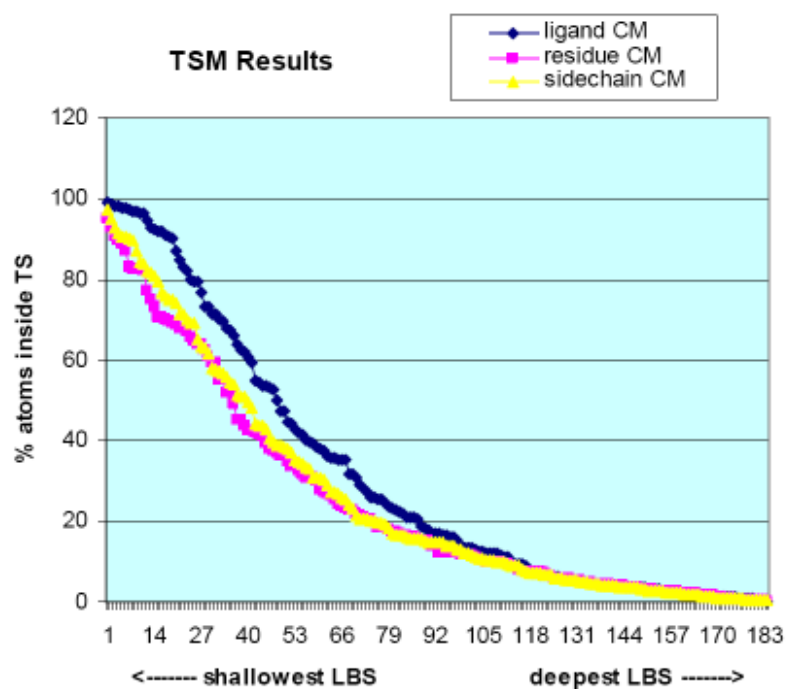


Figure 4A

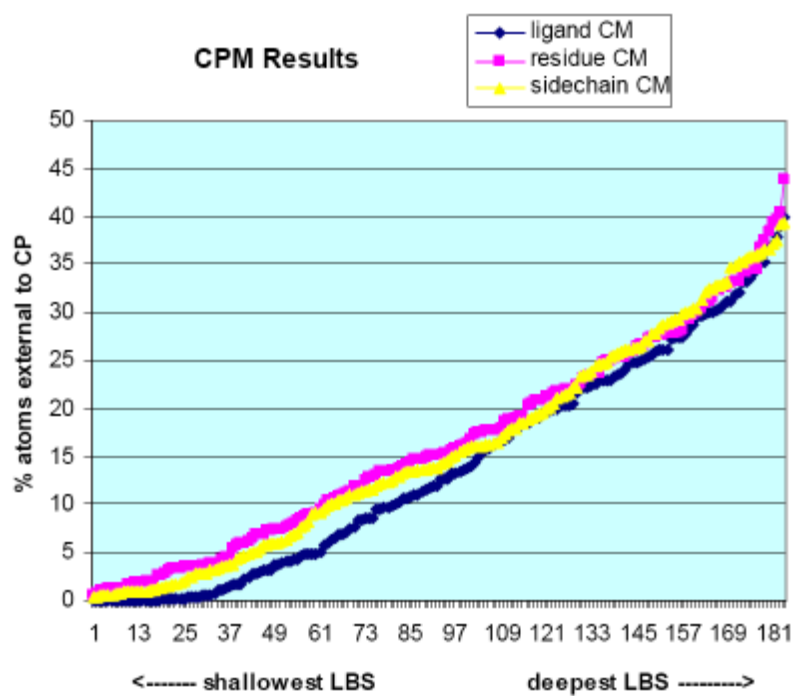


Figure 4B

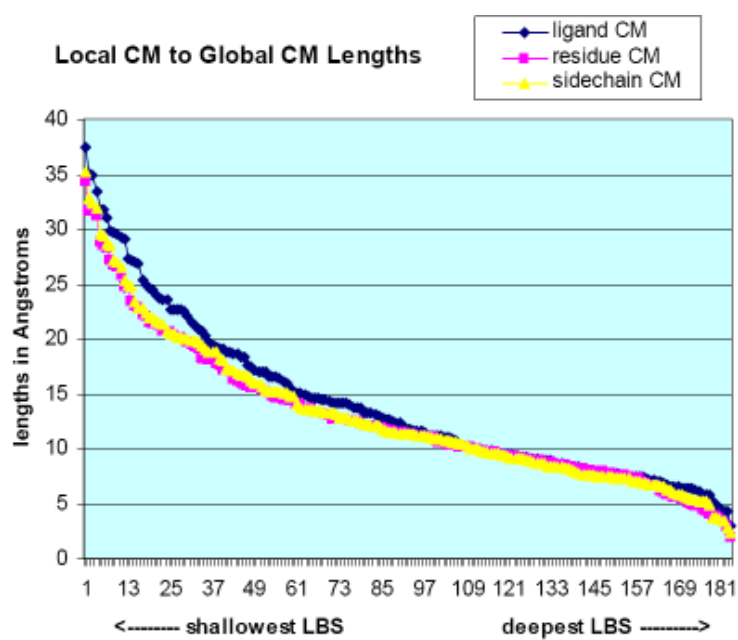


Figure 4C

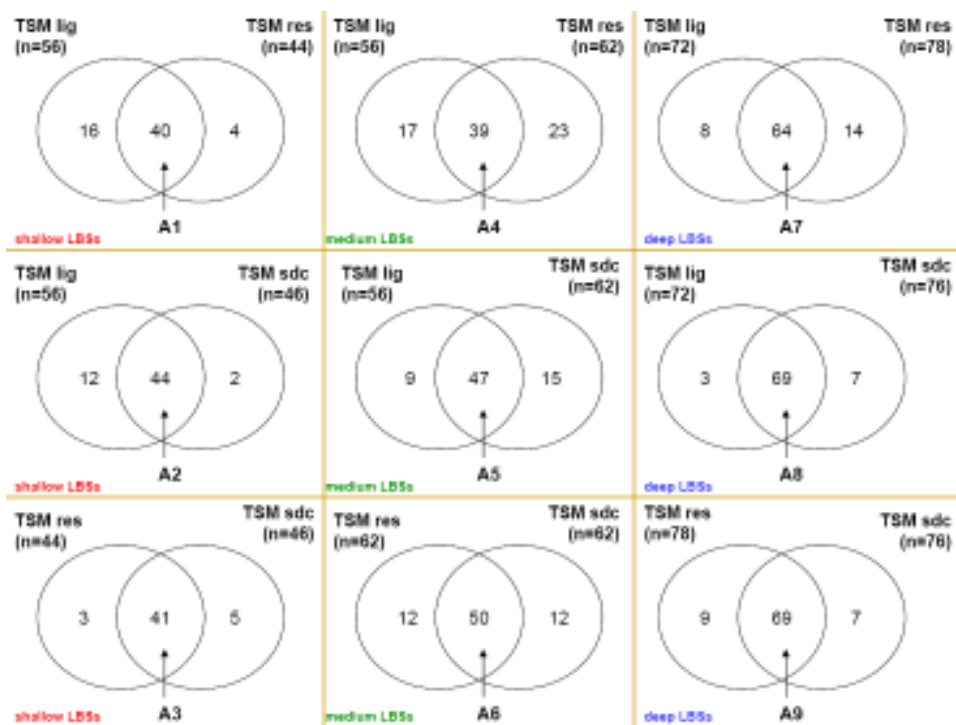


Figure 5A

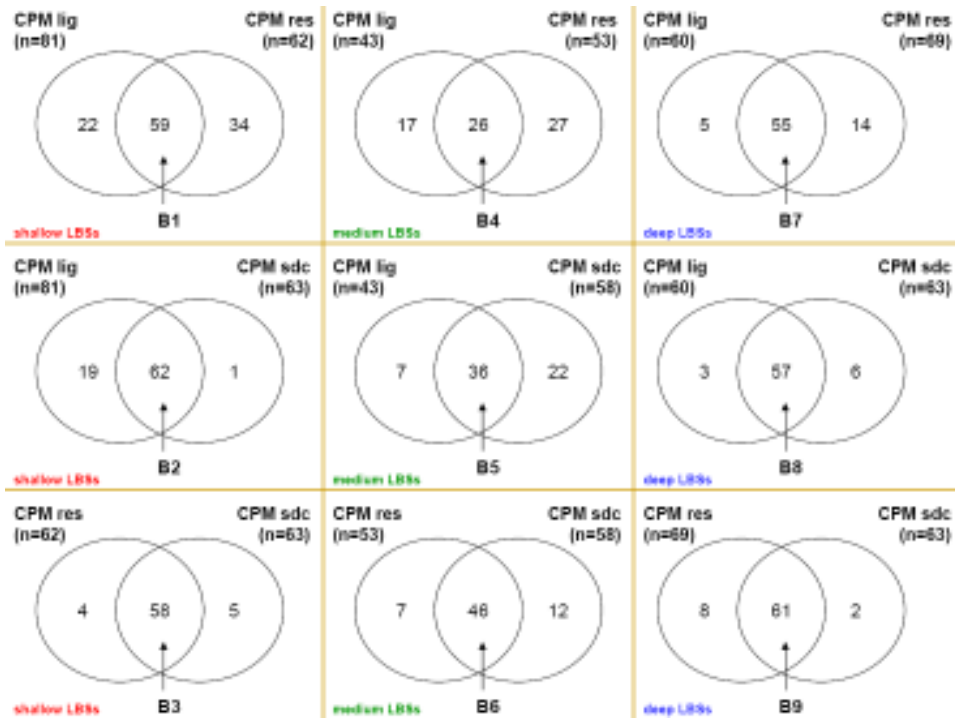


Figure 5B

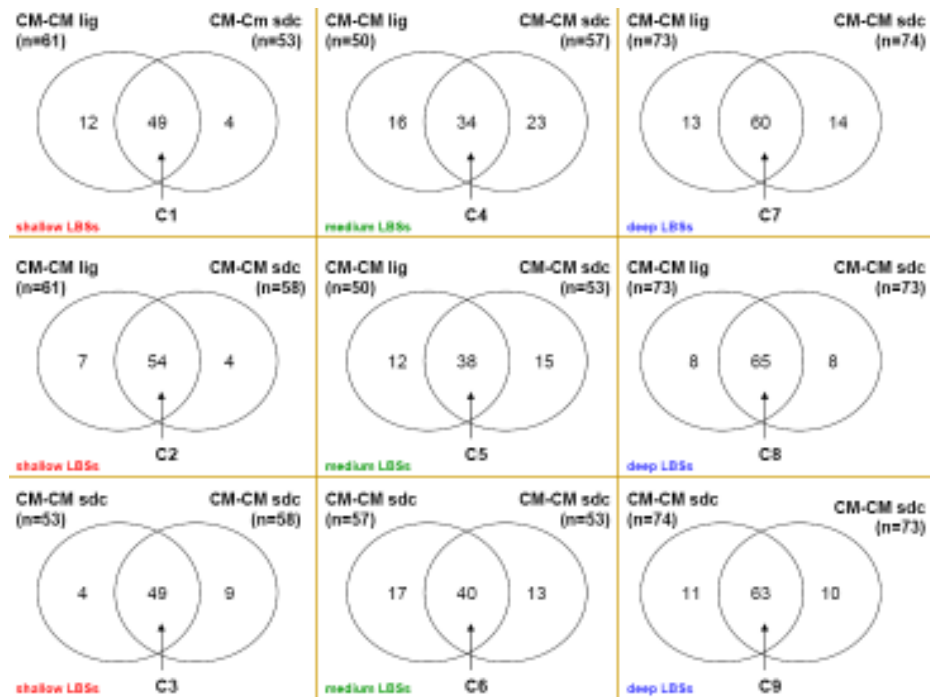


Figure 5C

TS method:

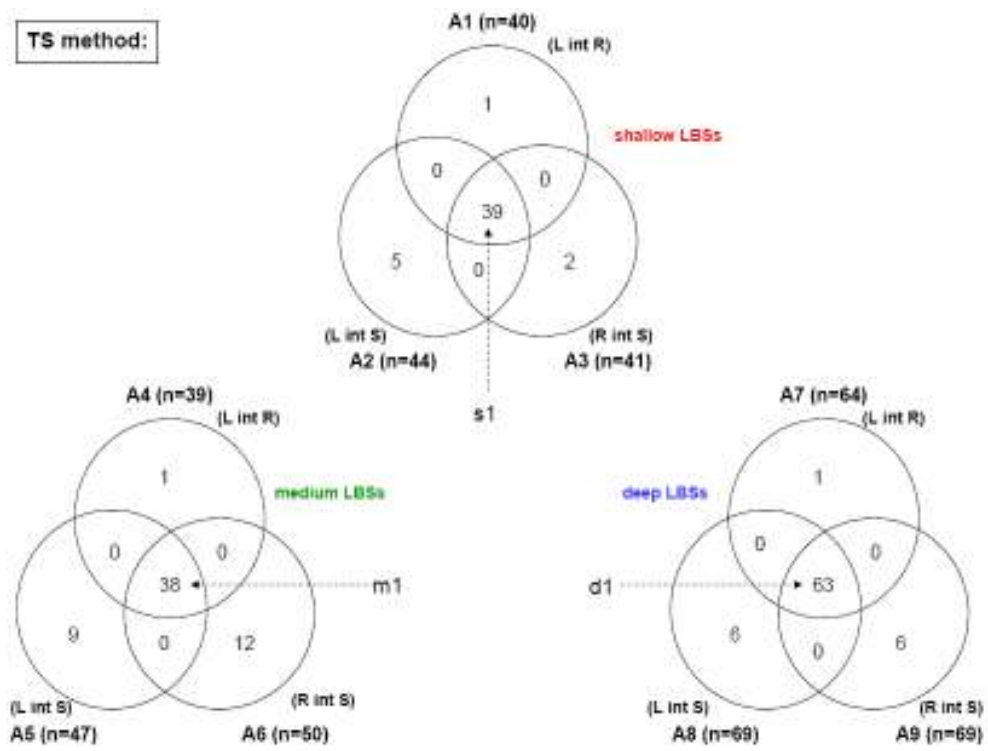


Figure 6A

CP method:

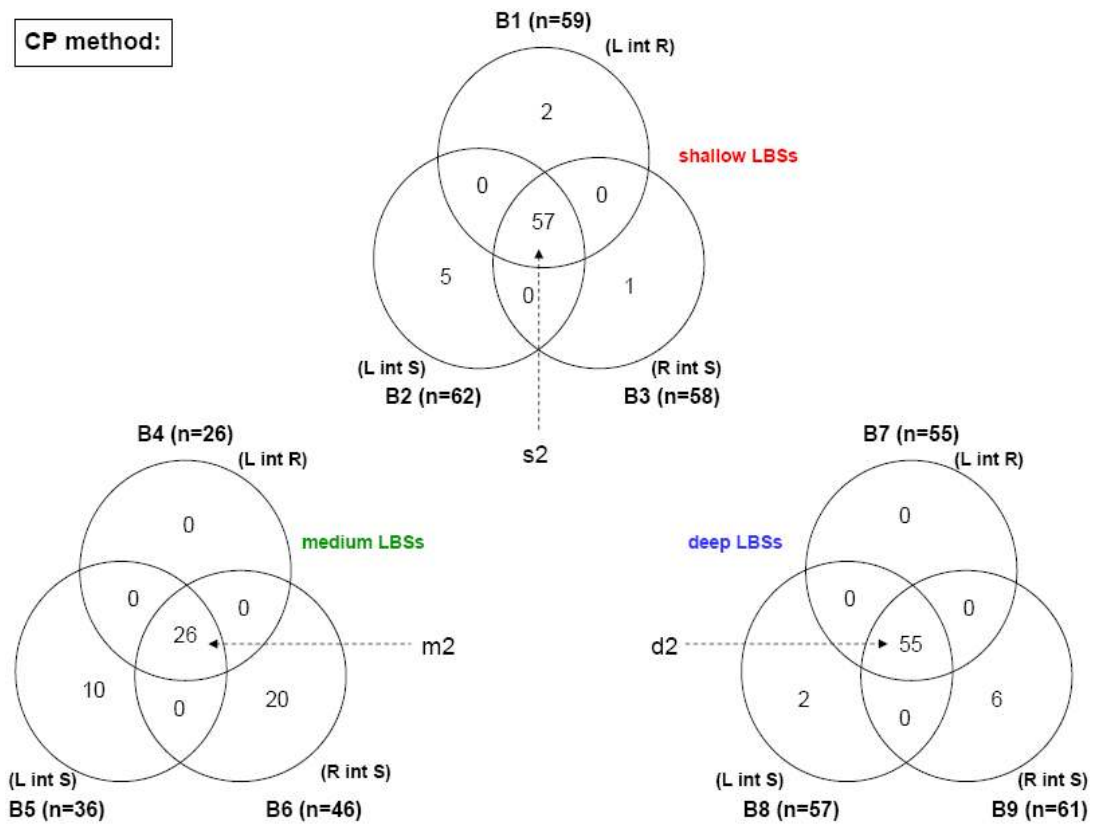


Figure 6B

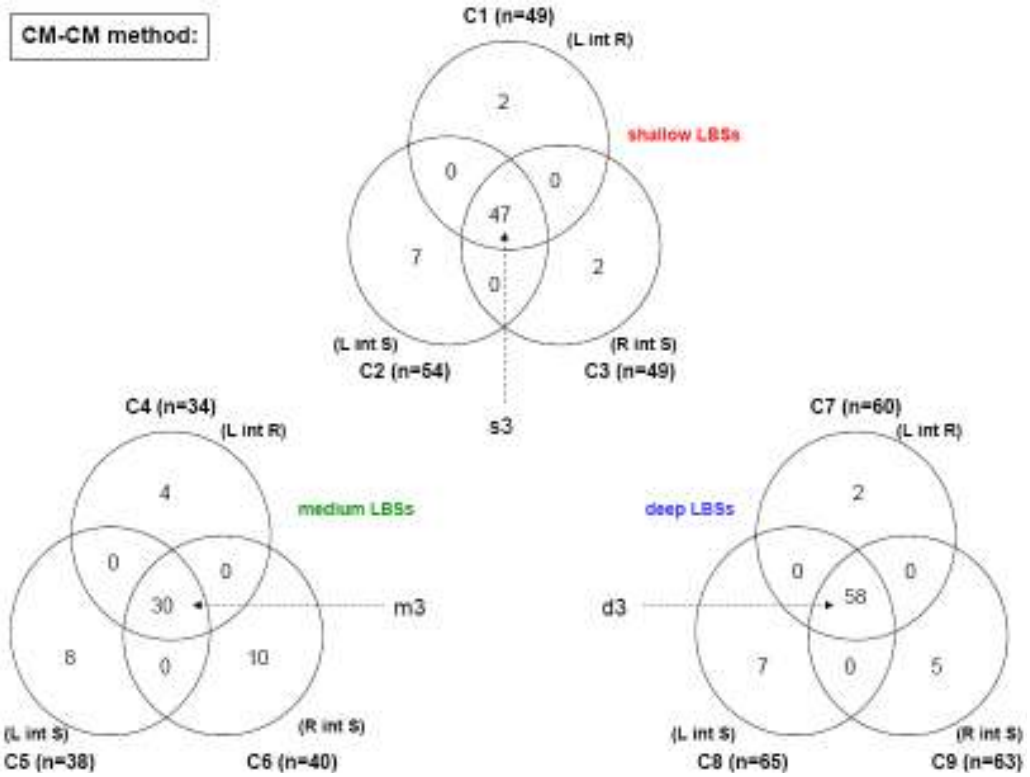


Figure 6C

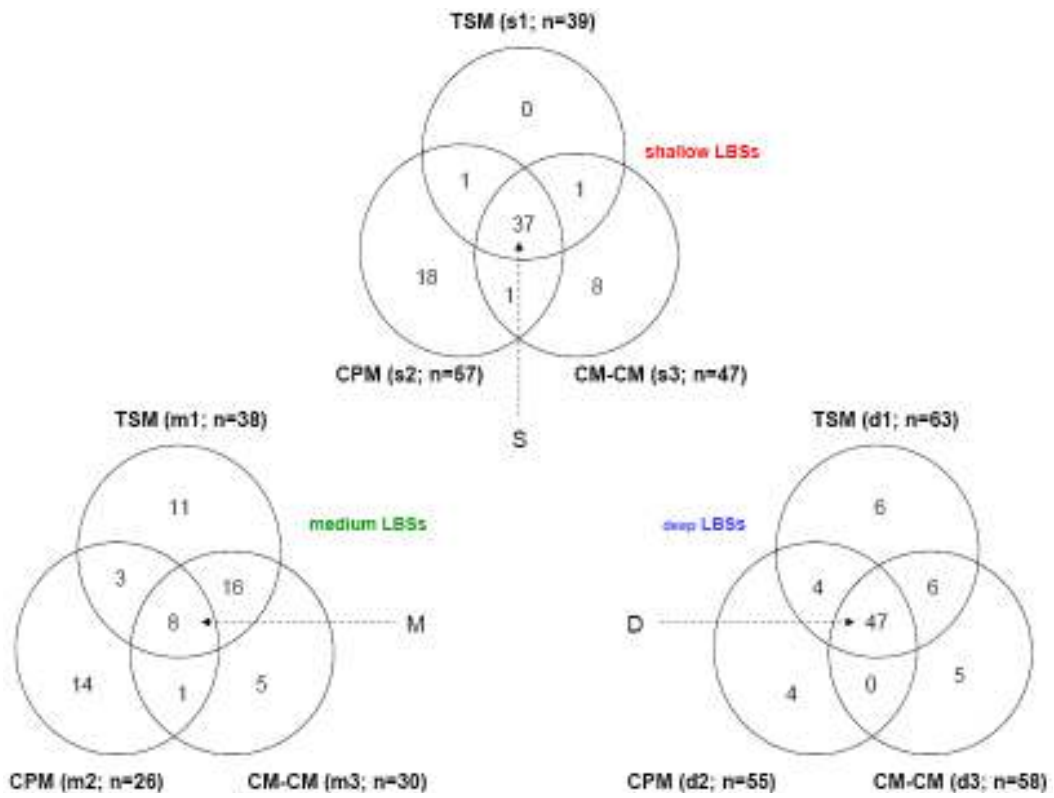


Figure 7A (CM-to-CM method included)

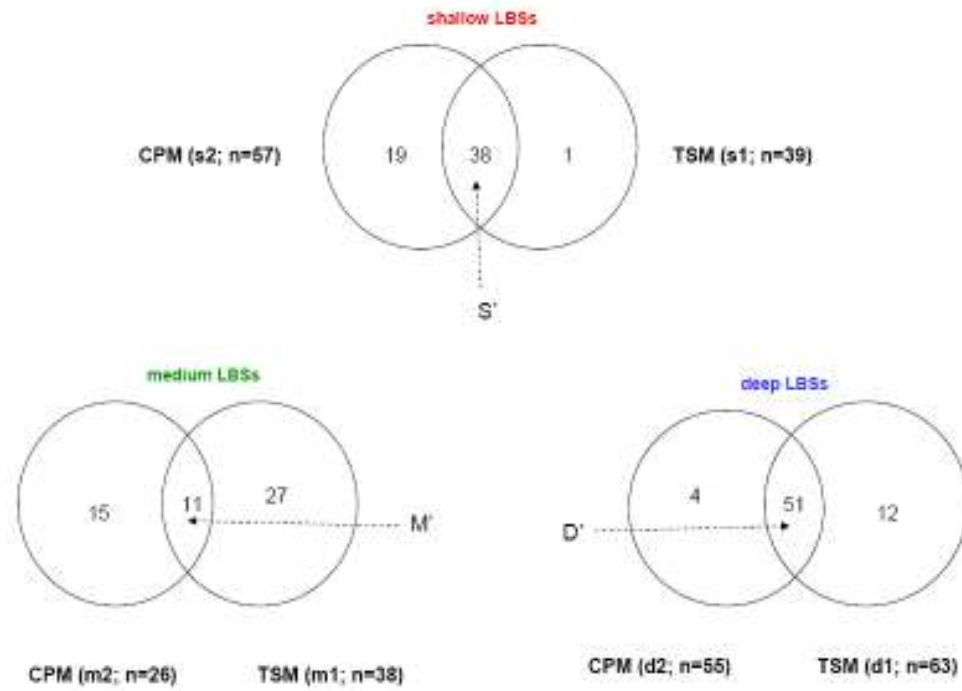


Figure 7B (CM-to-CM method excluded)

TABLES:

Table 1 (part 1 of 4)

Structure PDB ID	Shorthand designation	no. of domains	class	LIG # or LBS #	Ligand Name
1ADS	Aa	1	1	0	NAP-350
9ICD	Ab	1	1	0	NAP-1
1IPD	Ac	1	1	1	SO4-346
				2	SO4-347
1GOX	Ad	1	1	0	FMN-1
1TDE	Ae	2	1	0	FAD-500
1OYB	Af	1	1	1	FMN-401
				2	HBA-402
2NPX	Ag	3	1	1	FAD-448
				2	NAD-818
				3	CYO-42
1CCA	Ah	2	1	0	HEM-1
1ARP	Ai	2	1	1	HEM-345
				2	NAG-348
				3	NAG-349
1PBE	Aj	2	1	1	FAD-395
				2	PHB-396
1HMY	Ak	2	1	0	SAM-328
3CLA	Al	1	1	1	CLM-221
				2	CO-222
1GPB	Am	1	1	0	PLP-999
1ULA	An	1	1	1	SO4-290
				2	SO4-291
1STO	Ao	1	1	1	OMP-216
				2	OH-214
2YHX	Ap	3	1	0	OTG-1
1PHP	Aq	2	2	1	ADP-395
				2	MG-1
1GKY	Ar	2	1	1	5GP-187
				2	SO4-188
2CUT	As	1	1	0	DEP-401
1THG	At	1	1	1	NAG-990
				2	NAG-991
				3	NAG-994
				4	NAG-996
1RPA	Au	1	1	1	TAR-343
				2	NAG-344
				3	NAG-347
1RNH	Av	1	3	1	MSE-47
				2	MSE-50
				3	MSE-142
				4	SO4-156
1ONC	Aw	1	2	0	SO4-105
1FUT	Ax	1	2	0	2GP-108
1ROB	Ay	1	1	0	C2P-126
1SNC	Az	1	1	1	PTP-143
				2	CA-142

Table 1 (part 2 of 4)

1CDG	Ba	4	1	1	MAL-688
				2	MAL-689
				3	MAL-690
1BYB	Bb	1	1	1	GLC-496
				2	GLC-497
				3	GLC-498
				4	GLC-499
				5	SO4-880
1XNB	Bc	1	1	0	SO4-191
2SIM	Bd	1	2	0	DAN-800
1BYH	Be	1	1	1	BUT-215
				2	GLC-216
				3	GLC-217
1FMP	Bf	1	1	0	FMP-301
1BLL	Bg	2	1	1	ZN-488
				2	ZN-489
				3	LEU(I-1)
				4	FOR(I-2)
				5	VAL(I-3)
				6	VAL(I-4)
				7	ASP(I-5)
2CTC	Bh	2	1	1	LOF-309
				2	ZN-308
2GMT	Bi	2	1	0	HIN-247
1PPC	Bj	2	1	1	NAS(I-1)
				2	APH(I-3)
				3	PIP(I-4)
				4	GLY(I-2)
2ALP	Bk	2	1	1	SO4-1
				2	SO4-2
1ELA	Bl	2	1	1	TFA(B-256)
				2	ISO(B-259)
				3	SO4(B-290)
				4	ACY(B-300)
				5	LYS(B-257)
				6	PRO(B-258)
1HNE	Bm	2	3	1	ALM(I-5)
				2	MSU(I-1)
				3	ALA(I-2)
				4	ALA(I-3)
				5	PRO(I-4)
1PEK	Bn	2	1	1	PRO(C-1)
				2	ALA(C-2)
				3	PRO(C-3)
				4	PHE(C-4)
				5	ALA(D-5)
				6	ALA(D-6)
3SGA	Bo	2	1	1	PHA(P-1)
				2	ACE(P-5)
				3	PRO(P-4)
				4	ALA(P-3)
				5	PRO(P-2)

Table 1 (part 3 of 4)

1PIP	Bp	2	1	1	NIT(B-219)
				2	SIN(B-213)
				3	GLN(B-400)
				4	VAL(B-401)
				5	VAL(B-402)
				6	ALA(B-403)
				7	ALA(B-404)
1SMR	Bq	2	1	1	LPL(B-8)
				2	PIV(B-1)
				3	HIS(B-2)
				4	PRO(B-3)
				5	PHE(B-4)
				6	HIS(B-5)
				7	TYR(B-7)
				8	TYR(B-8)
				9	SER(B-9)
1PPI	Br	2	1	1	IVA(I-324)
				2	PLE(I-327)
				3	OPH(I-328)
				4	MAN-329)
				5	XYS-330)
				6	SO4-38)
				7	VAL(I-325)
				8	VAL(I-326)
3APR	Bs	2	1	1	FRD(I-5)
				2	PRO(I-2)
				3	PHE(I-3)
				4	HIS(I-4)
1EPM	Bt	2	1	1	PSA(I-1)
				2	SO4-1
				3	SO4-2
				4	SO4-3
				5	THR(I-5)
				6	PHE(I-4)
				7	GLN(I-3)
				8	ALA(I-2)
				9	LEU(I-2')
				10	ARG(I-3')
				11	GLU(I-4')
1MPP	Bu	2	1	0	SO4-501
1HYT	Bv	2	1	1	BZS-807
				2	DMS-808
				3	ZN-805
1IAG	Bw	1	1	1	SO4-260
				2	ZN-999
1ADD	Bx	1	3	1	IDA-353
				2	ZN-400
2DHC	By	1	3	0	DCE-600
1PII	Bz	2	1	1	PO4-453
				2	PO4-454
2DKB	Ca	2	1	1	PLP-272
				2	MES-434

Table 1 (part 4 of 4)

1CSH	Cb	1	1	1	AMX-700
				2	OAA-702
2FOR	Cc	1	1	1	OTE-545
				2	OTE-546
				3	OTE-547
				4	OTE-548
1CIL	Cd	1	2	1	ETS-262
				2	ZN-281
8ACN	Ce	3	3	1	NIC-755
				2	FS4-999
5ENL	Cf	2	1	1	2PG-442
				2	CA-438
1PDA	Cg	3	1	1	DPM-314
				2	ACY-315
1MNS	Ch	2	1	1	APG-166
				2	MG-360
3PGM	Ci	1	1	1	MP3-3
				2	SO2-2
				3	SO1-1
1BIB	Cj	3	1	0	BTN-500
2ABK	Ck	2	1	0	FS4-300
2ACK	Cl	1	1	0	EDR-999
2CND	Cm	2	1	0	FAD-271
2PGD	Cn	2	2	1	SO4-505
				2	SO4-507
				3	SO4-508
4BCL	Co	1	1	1	BCL-1
				2	BCL-2
				3	BCL-3
				4	BCL-4
				5	BCL-5
				6	BCL-6
				7	BCL-7

Tangent Sphere Method			Cutting Plane Method			CM-CM Method		
shallow	medium	deep	shallow	medium	deep	shallow	medium	deep
Ac.lbs1	Ab.lbs0	Aa.lbs0	Ab.lbs0	Al.lbs1	Aa.lbs0	Ab.lbs0	An.lbs2	Ad.lbs0
Ac.lbs2	Ak.lbs0	Bt.lbs7	Ac.lbs1	Ac.lbs1	Ad.lbs0	Ac.lbs1	As.lbs0	Ae.lbs0
Al.lbs2	An.lbs0	Bt.lbs8	Ac.lbs2	Be.lbs2	Ae.lbs0	Ac.lbs2	Au.lbs0	Br.lbs3
Al.lbs3	Aq.lbs1	Bv.lbs1	Al.lbs2	Bg.lbs1	Af.lbs1	Al.lbs2	Av.lbs4	Br.lbs7
Al.lbs2	Au.lbs2	Bv.lbs3	Ai.lbs3	Bg.lbs4	Af.lbs2	Ai.lbs3	Az.lbs1	Bs.lbs3
Al.lbs1	Ax.lbs0	Bx.lbs1	Al.lbs2	Bg.lbs5	Ag.lbs1	Al.lbs2	Be.lbs3	Bt.lbs1
At.lbs2	Az.lbs1	Bx.lbs2	Ao.lbs2	Bh.lbs1	Ag.lbs2	Al.lbs2	Be.lbs3	Bt.lbs7
At.lbs3	Bb.lbs4	By.lbs0	At.lbs1	Bj.lbs2	Ag.lbs3	At.lbs2	Bi.lbs0	Bv.lbs1
At.lbs4	Be.lbs3	Bz.lbs1	Al.lbs2	Bl.lbs1	Al.lbs1	At.lbs3	Bi.lbs2	Bv.lbs3
Au.lbs3	Bg.lbs2	Ca.lbs1	At.lbs3	Bl.lbs4	Aj.lbs1	At.lbs4	Bj.lbs2	Bx.lbs1
Av.lbs3	Bg.lbs3	Ca.lbs2	At.lbs4	Bm.lbs1	Aj.lbs2	Au.lbs3	Bj.lbs4	Bx.lbs2
Ba.lbs1	Bh.lbs1	Cb.lbs2	Au.lbs2	Bn.lbs4	Am.lbs0	Av.lbs3	Bm.lbs5	Ca.lbs1
Ba.lbs2	Bi.lbs0	Cd.lbs1	Au.lbs3	Bq.lbs3	An.lbs0	Ba.lbs1	Bn.lbs2	Ca.lbs2
Ba.lbs3	Bj.lbs2	Cd.lbs2	Av.lbs3	Br.lbs1	Ap.lbs0	Ba.lbs2	Bn.lbs6	Cb.lbs2
Bb.lbs5	Bj.lbs4	Ce.lbs1	Az.lbs1	Br.lbs3	Ar.lbs1	Ba.lbs3	Bo.lbs4	Cd.lbs1
Bc.lbs0	Bk.lbs1	Ce.lbs2	Ba.lbs1	Br.lbs8	Au.lbs1	Bb.lbs5	Bo.lbs5	Cd.lbs2
Bg.lbs7	Bl.lbs5	Cf.lbs1	Ba.lbs2	Bs.lbs2	Ar.lbs1	Bc.lbs0	Bp.lbs6	Ce.lbs1
Bm.lbs2	Bm.lbs5	Cf.lbs2	Ba.lbs3	Bs.lbs4	Av.lbs2	Bg.lbs1	Bp.lbs7	Ce.lbs2
Bn.lbs1	Bn.lbs2	Cg.lbs1	Bb.lbs5	Bt.lbs6	Au.lbs1	Bg.lbs2	Bq.lbs3	Cf.lbs1
Bo.lbs2	Bn.lbs3	Cg.lbs2	Bc.lbs0	Bt.lbs9	Av.lbs2	Bg.lbs3	Bq.lbs4	Cf.lbs2
Bo.lbs3	Bn.lbs6	Ch.lbs1	Be.lbs3	Bt.lbs9	Bb.lbs2	Bg.lbs4	Bq.lbs7	Cg.lbs1
Bp.lbs2	Bo.lbs5	Ch.lbs2	Bb.lbs3	Bv.lbs2	Bb.lbs3	Bg.lbs5	Bq.lbs8	Cg.lbs2
Bp.lbs3	Bp.lbs6	Ci.lbs1	Bj.lbs1	Bw.lbs1	Bf.lbs0	Bg.lbs6	Br.lbs1	Ch.lbs1
Bp.lbs4	Bp.lbs7	Ci.lbs2	Bk.lbs2	Bz.lbs2	Bh.lbs2	Bh.lbs2	Br.lbs2	Ci.lbs1
Bq.lbs9	Bq.lbs2	Cj.lbs0	Bl.lbs3	Cc.lbs2	Bh.lbs3	Bh.lbs3	Bs.lbs2	Ci.lbs2
Br.lbs6	Bq.lbs3	Cj.lbs1	Bl.lbs6	Cc.lbs3	Bh.lbs4	Bh.lbs4	Bs.lbs4	Ci.lbs3
Br.lbs2	Bq.lbs4	Ck.lbs0	Bm.lbs2	Cc.lbs4	Bh.lbs5	Bh.lbs5	Bt.lbs4	Ci.lbs4
Bt.lbs3	Br.lbs1	Cn.lbs1	Bm.lbs3	Ck.lbs0	Br.lbs2	Br.lbs2	Bt.lbs5	Ci.lbs5
Bt.lbs4	Bs.lbs2	Cn.lbs2	Bn.lbs1	Cn.lbs3	Br.lbs7	Br.lbs7	Bt.lbs6	Ci.lbs6
Bu.lbs0	Bs.lbs3	Co.lbs5			Bs.lbs1		Bt.lbs7	
Bv.lbs2	Bs.lbs4	Co.lbs7						
Bw.lbs1	Bt.lbs6							
Bz.lbs2	Bt.lbs9							
Cb.lbs2	Bw.lbs2							
Cc.lbs3	Bx.lbs2							
Cc.lbs1	Cb.lbs1							
Ck.lbs0	Cc.lbs2							
Cn.lbs0	Cc.lbs3							
Co.lbs1	Cc.lbs4							
	Cc.lbs5							
	Cc.lbs6							
	Cc.lbs7							
	Cc.lbs8							
	Cc.lbs9							
	Cc.lbs10							
	Cc.lbs11							
	Cc.lbs12							
	Cc.lbs13							
	Cc.lbs14							
	Cc.lbs15							
	Cc.lbs16							
	Cc.lbs17							
	Cc.lbs18							
	Cc.lbs19							
	Cc.lbs20							
	Cc.lbs21							
	Cc.lbs22							
	Cc.lbs23							
	Cc.lbs24							
	Cc.lbs25							
	Cc.lbs26							
	Cc.lbs27							
	Cc.lbs28							
	Cc.lbs29							
	Cc.lbs30							
	Cc.lbs31							
	Cc.lbs32							
	Cc.lbs33							
	Cc.lbs34							
	Cc.lbs35							
	Cc.lbs36							
	Cc.lbs37							
	Cc.lbs38							
	Cc.lbs39							
	Cc.lbs40							
	Cc.lbs41							
	Cc.lbs42							
	Cc.lbs43							
	Cc.lbs44							
	Cc.lbs45							
	Cc.lbs46							
	Cc.lbs47							
	Cc.lbs48							
	Cc.lbs49							
	Cc.lbs50							
	Cc.lbs51							
	Cc.lbs52							
	Cc.lbs53							
	Cc.lbs54							
	Cc.lbs55							
	Cc.lbs56							
	Cc.lbs57							
	Cc.lbs58							
	Cc.lbs59							
	Cc.lbs60							
	Cc.lbs61							
	Cc.lbs62							
	Cc.lbs63							
	Cc.lbs64							
	Cc.lbs65							
	Cc.lbs66							
	Cc.lbs67							
	Cc.lbs68							
	Cc.lbs69							
	Cc.lbs70							
	Cc.lbs71							
	Cc.lbs72							
	Cc.lbs73							
	Cc.lbs74							
	Cc.lbs75							
	Cc.lbs76							
	Cc.lbs77							
	Cc.lbs78							
	Cc.lbs79							
	Cc.lbs80							
	Cc.lbs81							
	Cc.lbs82							
	Cc.lbs83							
	Cc.lbs84							
	Cc.lbs85							
	Cc.lbs86							
	Cc.lbs87							
	Cc.lbs88							
	Cc.lbs89							
	Cc.lbs90							
	Cc.lbs91							
	Cc.lbs92							
	Cc.lbs93							
	Cc.lbs94							
	Cc.lbs95							
	Cc.lbs96							
	Cc.lbs97							
	Cc.lbs98							
	Cc.lbs99							
	Cc.lbs100							

Table2

Table 3A: Deep LBSs

STRUCTURE	T.S. Method				C.P. Method				CM-to-CM Method			
	lig	res	sdv	ave	lig	res	sdv	ave	lig	res	sdv	ave
Aa.lbs0	9.5105	6.3271	6.5261	7.45457	20.2547	21.9260	25.5074	22.5627	10.28162	9.04634	9.14596	9.49131
Ad.lbs0	1.4079	0.2594	1.0745	0.91393	32.1230	34.4943	30.0482	32.2218	5.74836	3.76268	5.18857	4.89987
Ae.lbs0	1.0204	3.8776	5.4762	3.45807	39.8639	34.1497	35.2041	36.4059	5.25637	8.20853	9.05430	7.50640
Af.lbs1	1.3371	0.6171	0.3343	0.76283	29.8534	33.2219	35.8961	32.9905	5.89282	4.77545	3.65929	4.77585
Af.lbs2	2.0057	2.4428	2.2885	2.24567	26.1764	26.5107	26.1507	26.2793	7.02114	7.35308	7.24344	7.20589
Ag.lbs1	2.6075	7.3639	2.2063	4.05923	33.2092	25.7307	32.8940	30.6113	8.99809	12.47014	8.62754	10.03190
Ag.lbs2	2.0057	3.3238	0.5444	1.95797	24.8424	25.2149	35.9312	28.6628	8.42256	9.70094	6.20813	8.10888
Ag.lbs3	0.8309	2.1490	1.8082	1.59503	28.6533	27.6218	25.9885	27.4212	6.76621	8.49437	8.31799	7.85952
Ai.lbs1	1.3387	0.7302	5.2333	2.43407	30.1014	30.9533	22.1907	27.7485	6.40161	5.44434	8.79111	6.87902
Aj.lbs1	1.0975	2.5178	0.8070	1.47410	30.2776	27.1768	34.7321	30.7295	6.36432	7.77716	5.88053	6.67400
Am.lbs0	0.8071	1.7486	1.2106	1.25543	39.0823	37.4682	39.2617	38.6041	6.52328	8.84403	7.43424	7.60052
An.lbs1	4.3401	4.0301	3.7201	4.03010	23.4278	21.9221	24.7564	23.3688	7.82188	7.48854	7.27156	7.52733
Ap.lbs0	2.2796	0.6079	1.0030	1.29683	27.3860	33.2827	34.8328	31.8338	7.47939	4.51663	5.34812	5.78005
Aq.lbs2	4.6210	2.5931	3.6569	3.62367	25.9641	31.5160	27.8590	28.4464	9.72327	7.86723	8.93589	8.84213
Ar.lbs1	2.8986	4.4859	4.3478	3.91077	31.1249	25.3968	26.2940	27.6052	6.36456	7.57155	7.43626	7.12412
Au.lbs1	6.2634	5.2255	3.5075	4.99880	24.8032	26.5927	27.8096	26.4018	9.01569	8.48317	7.52633	8.34173
Av.lbs1	6.6836	8.4602	2.7073	5.95037	22.1658	22.5042	29.1878	24.6193	7.76219	8.21716	5.73234	7.23723
Av.lbs2	2.7919	1.1844	0.4230	1.46643	23.0118	28.2572	36.2098	29.1596	5.77724	4.04717	2.80917	4.21119
Eb.lbs2	1.9873	0.3057	1.7070	1.33333	25.0955	38.4968	30.4713	31.3545	7.25613	3.90801	6.66775	5.94396
Eb.lbs3	3.2611	3.2611	1.7580	2.76007	23.2357	25.4268	28.3057	25.6561	8.39079	8.33648	6.79967	7.84231
Ef.lbs0	4.0208	0.6149	2.3652	2.33363	22.2327	34.5790	24.4560	27.0892	7.39599	4.26679	5.90191	5.85490
Ek.lbs2	7.0434	4.8321	5.9787	5.95140	22.5225	25.0205	24.5700	24.0377	9.25730	8.09097	8.61611	8.65479
El.lbs1	2.2700	1.9116	2.1505	2.11070	25.6472	27.8773	25.3286	26.2844	6.58757	6.10394	6.51448	6.40200
Er.lbs2	2.4473	2.4051	1.2658	2.03940	27.1730	27.8481	33.0380	29.3530	6.55463	6.49278	4.89134	5.97958
Er.lbs7	6.3713	5.7384	3.5021	5.20393	21.6456	22.0253	25.6540	23.1083	9.07211	8.79786	7.60733	8.49243
Et.lbs1	2.9720	1.5906	3.4324	2.66500	23.6919	29.2591	21.2641	24.7384	7.13280	5.43769	7.53525	6.70191
Et.lbs7	5.9021	2.6789	2.5952	3.72540	20.3851	27.5848	29.3428	25.7709	8.98414	6.91482	6.60925	7.50274
Ev.lbs1	5.7014	5.2912	4.7170	5.23653	20.5906	20.8368	23.3798	21.6024	8.50683	8.21531	7.84664	8.18966
Ew.lbs3	4.1838	2.2149	4.0607	3.48647	22.3134	28.0148	23.4208	24.5830	7.45971	5.76439	7.34854	6.85755
Ex.lbs1	3.7966	5.9456	2.4713	4.07117	27.5072	25.0000	30.3367	27.6146	7.71042	9.08760	6.76607	7.85470
Ex.lbs2	0.9670	0.2865	0.5731	0.60887	35.2436	40.4370	37.5716	37.7507	4.39819	2.90809	3.76015	3.68881
Ez.lbs1	4.9092	4.9943	3.3201	4.40787	34.0806	34.0522	36.4926	34.8751	9.43109	9.46442	8.34145	9.07899
Ca.lbs1	1.2915	0.9343	0.7688	0.68153	31.9803	39.3296	35.7319	35.6806	6.26963	5.01368	5.39555	5.59962
Ca.lbs2	3.6593	0.7688	1.6913	2.03980	21.9557	30.3813	23.9545	25.4305	8.53387	5.59405	6.82265	6.98359
Cb.lbs2	3.0964	1.7104	2.0643	2.29037	28.3102	32.2029	29.8437	30.1189	7.74503	6.52315	6.73587	7.00135
Cd.lbs1	5.0490	2.5000	1.5196	3.02237	22.9902	25.9314	29.3627	26.0948	7.71650	6.02835	5.25182	6.33222
Cd.lbs2	0.3922	0.1471	0.2451	0.26147	36.8137	43.7745	39.4118	40.0000	3.02225	1.90705	2.35654	2.42861
Ce.lbs1	0.4818	0.4129	0.6710	0.52190	37.8871	39.6937	37.0440	38.2083	4.94249	4.78547	5.51390	5.08062
Ce.lbs2	1.1700	1.5485	1.0840	1.26750	33.2416	34.6008	35.1858	34.3427	7.15173	7.85439	6.95883	7.32165
Cf.lbs1	1.6418	0.3040	1.0033	0.98303	30.7692	36.7893	32.5023	33.3536	6.17896	3.82368	5.29381	5.09882
Cf.lbs2	2.7668	2.5236	2.7364	2.67560	30.0091	32.2894	31.2861	31.1949	7.66465	7.38576	7.58245	7.54429
Cg.lbs1	3.6080	7.4388	4.4543	5.16703	24.0535	21.9154	21.4699	22.4796	7.89290	9.95957	8.60208	8.81818
Cg.lbs2	3.3853	2.8953	4.0535	3.44470	26.1470	30.0668	26.5033	27.5724	7.76433	7.26717	8.37459	7.80203
Ch.lbs1	3.5582	4.2624	3.5582	3.79292	29.6887	31.1712	32.1720	31.0106	7.74771	8.30537	7.75728	7.93679
Ch.lbs2	5.0037	9.3773	5.9674	6.78230	30.4299	27.8354	30.0964	29.4539	8.68576	10.66112	9.13461	9.49383
Ci.lbs1	3.7643	5.0736	3.8734	4.23710	26.1866	23.2406	24.6590	24.6954	6.83944	7.64921	6.97797	7.15554
Ci.lbs2	1.2002	3.6552	0.4910	1.78213	34.8063	26.6776	36.5521	32.6787	4.56176	6.72447	3.38018	4.88880
Cl.lbs0	2.3637	1.9296	1.4231	1.90547	27.4964	32.5856	28.9918	29.6913	7.44867	6.97387	6.32670	6.91641
Cn.lbs2	4.0219	3.5021	2.6539	3.39263	29.4938	33.0506	33.1874	31.9106	9.04226	8.51375	7.64118	8.39906
Co.lbs5	0.0000	2.0956	0.4412	0.84560	37.0956	23.6765	32.4265	31.0662	4.25437	9.73766	7.64564	7.21256
Co.lbs6	0.6618	4.5588	4.5221	3.24757	33.4926	27.3897	26.0662	28.9828	8.18778	11.55079	11.54632	10.42830

Table 3B: Medium LBSs

STRUCTURE	T.S. Method				C.P. Method				CM-to-CM Method			
	lig	res	sdv	ave	lig	res	sdv	ave	lig	res	sdv	ave
Bh.lbs1	11.8755	17.4857	14.6192	14.6601	17.0352	13.5135	14.2735	14.9741	11.13238	12.69575	12.08921	11.9724
Ej.lbs2	16.9201	23.5727	13.9963	18.1297	14.9171	13.3824	18.9687	15.7561	10.70093	12.09912	10.00316	10.9342
Eq.lbs3	22.5010	11.4695	18.1203	17.3636	10.5934	14.7352	11.4695	12.2660	14.20903	11.40287	13.25944	12.9571
Er.lbs1	16.2447	16.4979	14.7257	15.8228	14.4304	17.5105	16.4979	16.1463	12.38781	12.48107	12.06181	12.3102
Es.lbs2	17.0459	11.5019	11.9983	13.5154	12.6189	18.8664	17.9975	16.4943	12.80356	11.17469	11.34710	11.7751
Et.lbs6	17.6643	18.3759	19.9665	18.6689	13.5622	17.7062	16.2411	15.8365	12.93160	13.06783	13.44475	13.1481
Et.lbs9	12.1808	11.4274	10.0879	11.2320	10.7576	15.8644	16.4923	14.3714	11.49769	11.28031	10.79240	11.1901
Ew.lbs2	18.5185	16.2346	20.6790	18.4774	11.0494	15.2469	11.1728	12.4897	11.17028	10.58626	11.55117	11.1026
Ch.lbs1	35.4173	22.6482	37.7470	31.9375	13.2409	16.1014	12.8281	14.0568	18.28575	15.51547	18.79482	17.5320
Cc.lbs1	15.3501	13.6894	20.4219	16.4871	15.5745	16.8761	13.8689	15.4398	14.21990	13.62440	15.15508	14.3331
Co.lbs2	22.8309	21.2868	15.7353	19.9510	16.2868	14.9632	18.4559	16.5686	16.57206	16.28053	15.09326	15.9819

Table 3C: Shallow LBSs

STRUCTURE	T.S. Method				C.P. Method				CM-to-CM Method			
	lig	res	sdv	ave	lig	res	sdv	ave	lig	res	sdv	ave
Ac.lbs1	67.5290	48.9961	51.3513	55.9588	0.6564	3.9382	3.2046	2.59973	22.61821	19.74564	20.04670	20.8035
Ac.lbs2	81.9305	59.3050	62.7027	67.9794	0.1158	1.8147	1.3900	1.10683	24.89007	21.42218	21.93579	22.7493
Ai.lbs2	86.8560	68.7221	76.5112	77.3631	0.0811	3.8540	1.7039	1.87967	25.36921	21.32868	22.85914	23.1857
Ai.lbs3	91.7647	72.9817	74.0365	79.5943	0.0000	1.2170	0.8925	0.70317	27.08570	22.09977	22.36949	23.8517
Al.lbs2	98.4760	92.8488	95.0762	95.4670	0.0000	1.6413	0.9379	0.85973	27.16972	24.73393	25.29898	25.7342
At.lbs1	90.2678	82.8172	90.6403	87.9084	0.6286	1.9558	0.9546	1.17967	29.30139	27.18628	29.48152	28.6571
At.lbs2	90.6403	89.1851	71.3620	73.7291	0.3027	4.4237	2.4680	2.39813	29.49389	23.00176	24.95588	25.8138
At.lbs3	98.1141	88.6380	90.3143	92.3555	0.1164	1.3098	1.0477	0.82263	33.37043	28.74042	29.35302	30.4880
At.lbs4	99.2317	94.9243	97.0664	97.0741	0.0698	1.2573	0.8947	0.73727	35.13666	31.21572	32.45906	32.9371
Au.lbs3	96.9936	82.7487	90.4438	90.0620	0.3937	2.8275	1.7538	1.65833	31.85904	26.68224	28.65107	29.0641
Av.lbs3	60.5753	69.7970	75.6345	68.6689	4.7377	2.0305	1.4382	2.73547	16.04120	17.21665	18.04765	17.1018
Ba.lbs1	91.8503	82.4848	83.8716	86.0689	1.6337	3.7234	3.3815	2.91287	34.87654	31.58646	31.91738	32.7935
Ba.lbs2	96.7325	90.7105	92.7622	93.4017	0.6459	2.0897	1.4628	1.39947	37.45268	34.36086	35.28394	35.6992
Ba.lbs3	83.0737	82.6268	87.0251	84.2452	2.8875	3.5334	2.7166	3.04583	31.74831	31.62383	32.87885	32.0837
Eb.lbs5	67.9236	43.9236	57.7580	56.5351	0.2038	1.9108	0.4586	0.85773	24.45640	20.55410	22.77531	22.5953
Ec.lbs0	97.9282	82.1823	74.9309	85.0138	0.0000	0.4834	0.8287	0.43737	20.89671	18.12214	17.23462	18.7478
Eg.lbs7	53.5948	51.5523	44.0632	49.7368	5.9913	6.1547	8.2244	6.79013	22.67510	22.27142	20.67289	21.8731
Em.lbs2	90.8924	77.0782	84.4743	84.1483	0.3667	2.0782	0.9780	1.14097	21.18420	19.04630	20.07942	20.1033
En.lbs1	71.1596	54.6581	50.7929	58.8702	0.1982	3.7661	3.5679	2.51073	18.79190	17.07170	16.63080	17.9817
Bo.lbs2	92.3749	64.6545	69.0220	75.2508	0.0794	3.4184	2.8594	2.11807	19.41146	15.52336	16.04409	16.9930
Bo.lbs3	79.4281	65.6871	55.6791	66.9314	1.5091	3.8920	4.6863	3.36247	17.07288	15.62567	14.70304	15.8005
Ep.lbs2	96.1934	63.6858	79.2145	79.6979	0.0000	3.2628	0.6042	1.28900	23.57125	17.58167	19.66017	20.2710
Ep.lbs3	94.6224	60.7251	80.8459	78.7311	0.0000	3.6254	0.6042	1.40987	22.70205	17.16216	19.85317	19.9058
Ep.lbs4	72.9909	51.6012	56.9184	60.5035	0.4834	4.4713	3.2628	2.73917	18.68024	16.06110	16.80683	17.1827
Eq.lbs9	40.3425	45.0816	49.5818	45.0020	1.0753	0.7965	0.4779	0.78323	17.47268	18.26699	18.83646	18.1920
Er.lbs4	84.9789	67.8903	69.9312	74.2335	0.1688	1.0549	1.0127	0.74547	24.67343	21.37890	21.69178	22.5814
Er.lbs6	79.5781	63.9662	71.5612	71.7018	0.1266	1.2236	0.4641	0.60477	23.53866	20.67673	21.98487	22.0668
Et.lbs2	97.7396	89.8702	91.3771	92.9956	0.0419	1.0465	0.6279	0.57210	29.67364	26.54252	27.09555	27.7706
Et.lbs3	80.0335	62.2436	65.1319	69.1363	0.0837	1.5906	1.0046	0.89297	23.99113	20.65617	21.31436	21.9872
Et.lbs4	69.4851	45.1235	58.1893	57.5973	1.0465	6.9067	2.8882	3.61380	22.03106	18.02183	19.96236	20.0051
Eu.lbs0	69.9014	84.7005	56.8613	60.4877	2.9189	7.9985	6.0273	5.64823	22.67629	20.07973	20.40709	21.0544
Ev.lbs2	66.4315	87.1616	89.8277	91.1403	0.0000	1.2715	0.8203	0.69727	29.81212	25.89404	26.62986	27.4420
Ew.lbs1	97.9012	70.1852	81.8519	83.3128	0.0000	3.3951	1.7901	1.72840	23.73275	18.22958	19.78687	20.5831
Ex.lbs2	62.4858	68.9841	63.1385	64.8695	6.8956	4.2849	6.6402	5.94023	26.79193	28.44772	26.98328	27.4076
Cc.lbs2	92.8187	70.4668	75.0898	79.4584	0.2693	3.4111	2.3339	2.00477	27.25275	22.81167	23.49499	24.5198
Cc.lbs3	97.3519	74.9102	82.2262	84.8294	0.0000	2.5583	1.1670	1.24177	29.04908	23.44567	24.82153	25.7721
Ck.lbs0	61.9676	67.1266	61.6077	63.5673	9.7181	8.3983	9.8980	9.33813	20.36178	21.22158	20.21158	20.5983
Cn.lbs3	76.6895	67.8523	68.9740	71.1719	1.2859	3.5021	3.6662	2.81807	31.08082	28.14889	28.44036	29.2234